MASARYKOVA UNIVERZITA
Přírodovědecká fakulta
Ústav teoretické fyziky a astrofyziky

Bakalářská práce

Brno 2024 Tomáš Pekárek

MASARYKOVA
UNIVERZITA
PŘÍRODOVĚDECKÁ FAKULTA
ÚSTAV TEORETICKÉ FYZIKY A ASTROFYZIKY

Semi-analytic modelling of jellysh galaxy orbits in clusters

Bakalářská práce

Tomáš Pekárek

Vedoucí práce: Mgr. Pavel Jáchym, Ph.D. **Brno 2024**

Bibliografický záznam

Autor:	Tomáš Pekárek Přírodovědecká fakulta, Masarykova univerzita Ústav teoretické fyziky a astrofyziky

Název práce:	Semi-analytické modelování drah galaktických medúz v kupách
Studijní program:	Fyzika
Studijní obor:	Astrofyzika
Vedoucí práce:	Mgr. Pavel Jáchym, Ph.D.
Akademický rok:	2023/2024
Počet stran:	VIII + 42
Klíčová slova:	kupy galaxií; vývoj galaxií; vnější dynamický tlak; medůzovité galaxie; oběžné dráhy galaxie; semi-analytické modelování; kupa galaxií Coma; galaxie NGC 4858; galaxie D100

Bibliographic Entry

Author:	Tomáš Pekárek Faculty of Science, Masaryk University

Title of Thesis:	Semi-analytic modelling of jellyfish galaxy orbits in clusters
Degree Programme:	Physics
Field of Study:	Astrophysics
Supervisor:	Mgr. Pavel Jáchym, Ph.D.
Academic Year:	2023/2024
Number of Pages:	VIII + 42
Keywords:	clusters of galaxies; evolution of galaxies; ram pressure stripping; jellyfish galaxies; galaxy orbits; semi-analytical modelling; Coma cluster; galaxy NGC 4858; galaxy D100

Abstrakt

Galaxie v kupách ovlivněné vnějším dynamickým tlakem – ram pressure stripping (RPS) poskytují v porovnání s běžnými galaxiemi navíc informaci o svém pohybu na obloze díky plynnému 'jellyfish' ohonu. Ten je tvořen materiálem, který byl z galaxie odstraněn působením vnějšího tlaku mezigalaktického plazmatu v kupách. Práce se zabývá studiem možných drah těchto galaktických medúz. K tomu jsme použili modely vytvořené pomocí numerické integrace drah těchto galaxií. Do modelů jsme dosadili parametry známé z pozorování a poté vytvářeli jednotlivé dráhy na základě změn volných, z pozorování neznámých parametrů. Na základě tvaru vymodelovaných drah a s pomocí předpovědí kosmologických simulací jsme vyhodnotili nejpravděpodobnější dráhy a dále jsme popsali závislosti RPS, celkové rychlosti a celkové vzdálenosti galaxií na čase. Modelování jsme provedli pro dvě galaxie z kupy Coma, NGC 4858 a D100.

Abstract

Galaxies in clusters influenced by ram pressure stripping (RPS) provide in comparison with 'regular' galaxies an additional information about their orbit on the sky thanks to the gas "jellyfish' tail. The tail is formed by material that has been removed from the galaxy by the external pressure of intergalactic plasma in clusters. This work deals with the study of possible orbits these jellyfish galaxies. We used models created with help of numerical integration of the orbits of these galaxies. Into the models we put parameters known from observations and then we modelled individual orbits based on a change of free parameters that are not known from obesrvations. Based on the shape of the modelled orbits and with help of the assumptions of cosmological simulations, we evaluated the most probable orbits and we also described dependencies of RP, deprojected velocity and deprojected distance on time. We did the modelling for two galaxies in the Coma cluster: NGC 4858 and D100.

MASARYKOVA UNIVERZITA
PŘÍRODOVĚDECKÁ FAKULTA
KOTLÁŘSKÁ 2, 611 37 BRNO
IČ: 00216224
DIČ: CZ00216224

ZADÁNÍ BAKALÁŘSKÉ PRÁCE

Akademický rok: 2023/2024

Ústav:	Ústav teoretické fyziky a astrofyziky
Student:	Tomáš Pekárek
Program:	Fyzika
Specializace:	Astrofyzika

Ředitel *ústavu* PřF MU Vám ve smyslu Studijního a zkušebního řádu MU určuje bakalářskou práci s názvem:

Název práce:	Semi-analytické modelování drah galaktických medúz v kupách
Název práce anglicky:	Semi-analytic modeling of jellyfish galaxy orbits in clusters
Jazyk závěrečné práce:	angličtina

Oficiální zadání:

Galaxie ovlivněné dynamickým tlakem mezigalaktického plynu v kupách galaxií poskytují v porovnání s běžnými galaxiemi navíc informace o svém pohybu na obloze – asymetrie plynného disku či rozložení plynu odstraněného z galaxií naznačují směr jejich oběhu kupou. Pomocí semi-analytického modelování lze provést analýzu možných drah. Ty musí být v souladu s pozorovanými parametry – radiální rychlostí galaxie (vůči kupě) a její polohou na obloze (vzhledem ke středu kupy). Naopak volnými parametry modelu jsou radiální vzdálenost galaxie (vzhledem k rovině centra kupy) a velikost složky rychlosti na obloze. V modelu bude pro gravitační potenciál kupy použit Navarro-Frenk-Whiteův (NFW) profil. Pomocí numerického integrování pohybové rovnice testovací částice v potenciálu kupy bude prozkoumán široký rozsah hodnot volných parametrů a odpovídající „rodiny" drah budou vyhodnoceny s ohledem na další argumenty (disperse rychlosti galaxií v kupě, očekávané první přiblížení galaxie do centra kupy, pozorovaný efekt působení dynamického tlaku na galaxii atp.). Model bude aplikován na galaxie pozorované v blízké kupě galaxií Coma (v souhvězdí Vlasů Bereniky). Tzv. galaktické medúzy procházejí silným vývojem v důsledku interakce s okolním mezigalaktickým plynem. Dynamický tlak okolního prostředí dokáže z galaxií odstranit jejich mezihvězdnou hmotu. Tím dochází k zastavení tvorby nových hvězd a galaxie se mění v pasivní rané typy. Odtržený materiál vytváří u galaxií jednostranné struktury, v nichž se galaktický plyn míchá s mezigalaktickým plynem. Doporučená literatura: - Press, W. H., Teukolsky, S. A., Vetterling, W. T., Flannery, B. P. (2007): Numerical Recipes: The Art of Scientific Computing, Cambridge University Press, ISBN:978-0521880688, http://numerical.recipes/book.html - Brilenkov, R., Eingorn, M., Zhuk, A. (2015): Dark and visible matter distribution in Coma cluster: theory vs observations, DOI: 10.48550/arXiv.1507.07234 - Fossati M., Gavazzi G., Boselli A., Fumagalli M. (2012): 65 kpc of ionized gas trailing behind NGC 4848 during its first crossing of the Coma cluster, Astronomy & Astrophysics, Volume 544, id.A128, 6 pp., DOI: 10.1051/0004-6361/201219933 - Köppen, J., Jáchym, P., Taylor, R., Palouš, J. (2018): Ram pressure stripping made easy: an analytical approach, Monthly Notices of the Royal Astronomical Society, Volume 479, Issue 4, p.4367-4390, DOI: 10.1093/mnras/sty1610 - Jáchym, P., Sun, M., Kenney, J. D. P., Cortese, L., Combes, F., Yagi M., Yoshida M, Palouš, J., Roediger, E. Molecular Gas Dominated 50 kpc Ram Pressure Stripped Tail of the Coma Galaxy D100. The Astrophysical Journal, Volume 839, Issue 2, article id. 114, 15 pp. (2017). DOI: 10.3847/1538-4357/aa6af5

Vedoucí práce:	Mgr. Pavel Jáchym, Ph.D.
Datum zadání práce:	13. 12. 2023
V Brně dne:	4. 4. 2024

Tomáš Pekárek, 13. 12. 2023
Mgr. Pavel Jáchym, Ph.D., 15. 12. 2023
RNDr. Luboš Poláček, 19. 12. 2023

Poděkování

Rád bych poděkoval především vedoucímu práce Mgr. Pavlu Jáchymovi, Ph.D. za trpělivost, cenné rady a odborné vedení. Dále děkuji Mgr. Filipu Hrochovi, Ph.D. za konzultace. Také bych chtěl poděkovat své rodině za podporu.

Prohlášení

Prohlašuji, že jsem svou bakalářskou práci vypracoval samostatně pod vedením vedoucího práce s využitím informačních zdrojů, které jsou v práci citovány.

Brno 13. května 2024 .....

Tomáš Pekárek

Contents

Chapter 1

Introduction

In this work, we will study galaxies in galaxy clusters that are influenced by ram pressure stripping. These galaxies provide in comparison with "regular" galaxies an additional information about their orbit. We have this information thanks to the ram pressure which removes interstellar medium from the galaxy and creates a "jellyfish tail" of removed material. The tail indicates the direction of motion of the galaxy in the plane of the sky. With the help of semi-analytical modelling, we will perform an analysis of possible trajectories of two jellyfish galaxies in the Coma cluster. These model trajectories have to be consistent with the observed orbital parameters of the galaxies: the line-of-sight velocity relative to the cluster mean, the projected position in the cluster, and the direction of the velocity component in the plane of the sky. In the model, we will use the Navarro-Frenk-White profile for gravitational potential of the cluster. With the help of numerical integration of the equation of motion of a test body in this potential, we will explore a wide range of free orbital parameters that are not known from observations (the line-of-sight position relative to the cluster center and the plane of the sky velocity), and we will try to constrain the orbits of the two galaxies.

Chapter 2

Galaxies

2.1 Clusters of galaxies

Galaxy clusters are one of the largest gravitationally bound objects in the Universe[1]. They are composed of galaxies, the intracluster medium (ICM) and dark matter. The ICM is a hot plasma emitting strong X-ray radiation, filling the space between the galaxies.

The typical composition of mass in a cluster is [2]:

$M_{\text{stars}} \approx 2\%$	stars and galaxies
$M_{\text{ICM}} \approx 13\%$	ICM
$M_{\text{DM}} \approx 85\%$	dark matter

Most baryons in clusters are in the ICM [3].

Galaxy clusters probably form from merging clumps of dark matter and their associated galaxies. The ICM is heated during the formation of the cluster [4]. There are two types of clusters. The first type is called poor clusters (or groups). Groups have dozens of galaxies and their diameter is about 1 Mpc. The second type are rich clusters. They have thousands of galaxies and their diameter is several Mpc [5]. A typical mass of a cluster is $\sim 10^{14} - 10^{15}\ M_{\odot}$ [6].

An example of a poor cluster is "our" Local group where the Milky Way galaxy takes place. Examples of rich clusters are the Virgo cluster (which is the closest rich cluster to us) or the Coma cluster. Galaxies in clusters may interact (e.g., the Antennae) [7].

[1] https://cfa.harvard.edu/research/topic/galaxy-clusters
[2] https://pages.aip.de/pfrommer/Lectures/clusters.pdf
[3] https://www.astro.princeton.edu/~burrows/classes/204/galaxy.cluster.pdf
[4] https://chandra.harvard.edu/xray_sources/galaxy_clusters.html
[5] https://www.astro.princeton.edu/~burrows/classes/204/galaxy.cluster.pdf
[6] https://pages.aip.de/pfrommer/Lectures/clusters.pdf
[7] https://www.astro.princeton.edu/~burrows/classes/204/galaxy.cluster.pdf

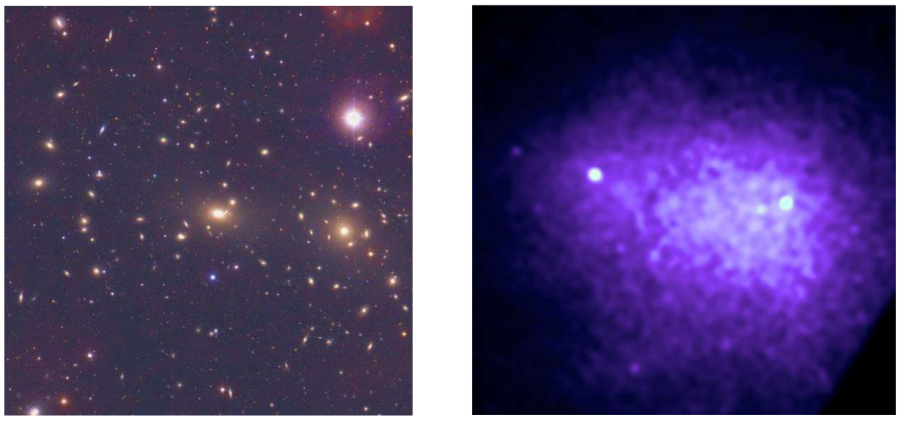

Figure 2.1: Comparison of Coma cluster in the optical (left) and X-rays (right), source: University of Hawaii

2.1.1 Coma cluster

The Coma cluster, which is also known as Abell 1656, is about 99 Mpc far away, it has redshift z = 0.0231 and contains more than 1000 galaxies. Two giant elliptical galaxies, NGC 4874 and NGC 4889, dominate the central region of the cluster. The Coma cluster has a mass about 10^{15} $M_{\odot}$. Approximately 10% of the mass of the Coma cluster represents the hot ionized ICM. The celestial size of the Coma cluster is more than 2° (Zadorozhna et al. 2023). Most of the galaxies in the central parts of the cluster are elliptical. In the outskirts, there are also younger spiral galaxies [8]. Fig. 2.1 shows the difference when the Coma cluster is observed in the optical and in X-rays. A composite view is then shown in Fig. 2.2, which combines XMM-Newton X-ray observations with an optical Sloan Digital Sky Survey (SDSS) image.

Figure 2.2: Coma cluster in X-ray and optical. Credit: ESA/XMM-Newton/SDSS/J. Sanders et al. 2019

[8] https://science.nasa.gov/missions/hubble/hubbles-galaxies-with-knots-bursts

2.2 Evolution of galaxies

The environment is a very important factor in galaxy evolution (Boselli, Fossati, and Sun 2022). Galaxies that are in regions with high density have different evolution than the field galaxies. There are thus systematic differences between cluster and field galaxies. Rich environments of galaxy clusters are dominated by early-type galaxies. Moreover, also the late-type galaxies in clusters are different from those in the field, specifically, they have a lower gas content which reduces their star formation.

2.2.1 Perturbing mechanisms

Various perturbing mechanisms have been proposed to explain different evolution of galaxies in high density regions (Boselli, Fossati, and Sun 2022). We can divide these mechanisms into two main families - gravitational perturbations with other members of cluster and hydrodynamic interaction.

The hydrodynamic interaction concerns the hot intracluster medium and cold interstellar medium (ISM). This interaction can remove the ISM from the galaxy. This is caused by external pressure which acts on the galaxy. The removal of the ISM by this external pressure is called ram pressure stripping (RPS).

The difference between these two families of perturbing mechanisms is that the gravitational interactions affect all components of a galaxy (dark matter, stars, gas, dust), while hydrodynamic interactions affect only the ISM.

RPS is considered as a main perturbing mechanism in nearby rich clusters (such as Coma or Virgo cluster). To decide what is the dominant perturbing mechanism in galaxies of different mass and belonging to different environments (from massive clusters to loose groups) at different time periods is difficult for example because the perturbing mechanisms are all active at the same time. It is still unclear what happens with the ISM stripped from the galaxy disc (more in section 2.3.2).

2.2.2 Green valley

Galaxies evolving from blue types which actively form stars to red ones which don't form stars, pass through the *green valley*. So the late-type galaxies are mostly blue, while early-type galaxies are mostly red because they contain old red stars.

In the *green valley* there are galaxies in which the star formation is quenching. Ram pressure stripping is one of the processes that quench star formation via the efficient removal of ISM. Fig. 2.3 shows the distribution of galaxies in the color-mass diagram clearly indicating the green valley transition population[9].

[9] https://astrobites.org/2022/03/23/sprinting-through-green-valley/

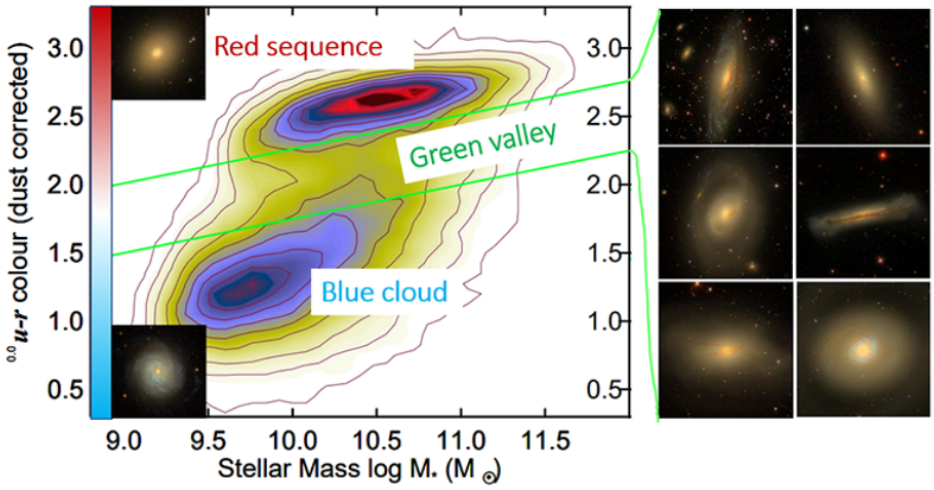

Figure 2.3: Galaxy color-mass diagram. Late-type galaxies actively forming stars are in the left lower corner, while passive early type galaxies are in the upper half of the diagram. Between them we can find the *green valley*. Examples of such transition galaxies are shown in the right. Source: Astrobites

2.3 Ram pressure stripping

In the last years the sensitivity of ground and space based observations and spectroscopic instruments is increasing and it allows astronomers to do large and deep multi-frequency surveys of local clusters - specifically Virgo and Coma. These large surveys have been complemented with extraordinary resolution of representative galaxies where astronomers can study in great detail the impact of the environment on their evolution. The increasing level of these observations requires corresponding level of theoretical and numerical models to interpret the observed data. So a new class of hydrodynamic simulations has been created, as well as semi - analytic models of galaxy formation. Thanks to the synergy of the observations and theoretical models, there has been important progress in the study of ram pressure stripping in recent years. A discovery of spectacular tails of at galaxies in some nearby clusters caused a growing interest of this mechanism (Boselli, Fossati, and Sun 2022).

2.3.1 The physical mechanism

The regions of high density, such as the galaxy clusters have a hot ($T_{ICM} \simeq 10^7 - 10^8$ K) and dense ($\rho_{\mathrm{ICM}} \simeq 10^{-3}\,\mathrm{cm}^{-3}$) ICM that is trapped in the gravitational potential well of the cluster. The galaxy which is moving in the cluster with the velocity V relative to the ICM experiences a drag force. This drag force exerts ram pressure. We can write the ram pressure as

$$P = \rho_{ICM} V^2, \tag{2.1}$$

where ρ_{ICM} is the density of ICM. The ram pressure can strip the gas component of ISM from the disk of the galaxy itself. Equation (2.1) shows that RP depends on the properties of the region and the motion of galaxy in this region. The effects of the ram pressure operating on a galaxy, i.e., stripping of the galaxy by ram pressure, depends on the physical properties of the galaxy. It is the gravitational restoring force of the galaxy that opposes the ram pressure. RPS may have radical consequences in dwarf galaxies where the gravitational forces are not sufficient to keep the ISM anchored in the stellar disc. So in this systems is the forming of stars quit at all (Gunn and Gott 1972).

RPS is a hydrodynamic interaction which occurs between ISM and ICM. Stars are not perturbed by RPS because they have too small cross section.

It is worth noting that RPS is a general process and do not have to be connected only with galaxies. There must be relative motion between an object and dense surroundings. So we can see it for example on stars (Mira).

2.3.2 Fate of the stripped gas

According to some observations and simulations, the stripped gas can either fall back on the galaxy disc or create long cometary tails (see examples in Boselli, Fossati, and Sun 2022). The gas can leave the galaxy only if it has velocity larger than is the escape velocity from the galaxy. This velocity is (for spherically symmetric body):

$$v_e = \sqrt{\frac{2GM_{\mathrm{DM}}}{r_{\mathrm{gas}}}}, \tag{2.2}$$

where M_{DM} is mass of the dark matter in the galaxy and r_{gas} is the distance of the gas from the nucleus of the galaxy. If this condition is not satisfied, the stripped gas will fall back on the galaxy disc, when the galaxy is in apocentre.

If the condition is satisfied the gas can create a long tail behind the galaxy - hence "jellyfish galaxy". An example of jellyfish galaxy is in Fig. 2.4.

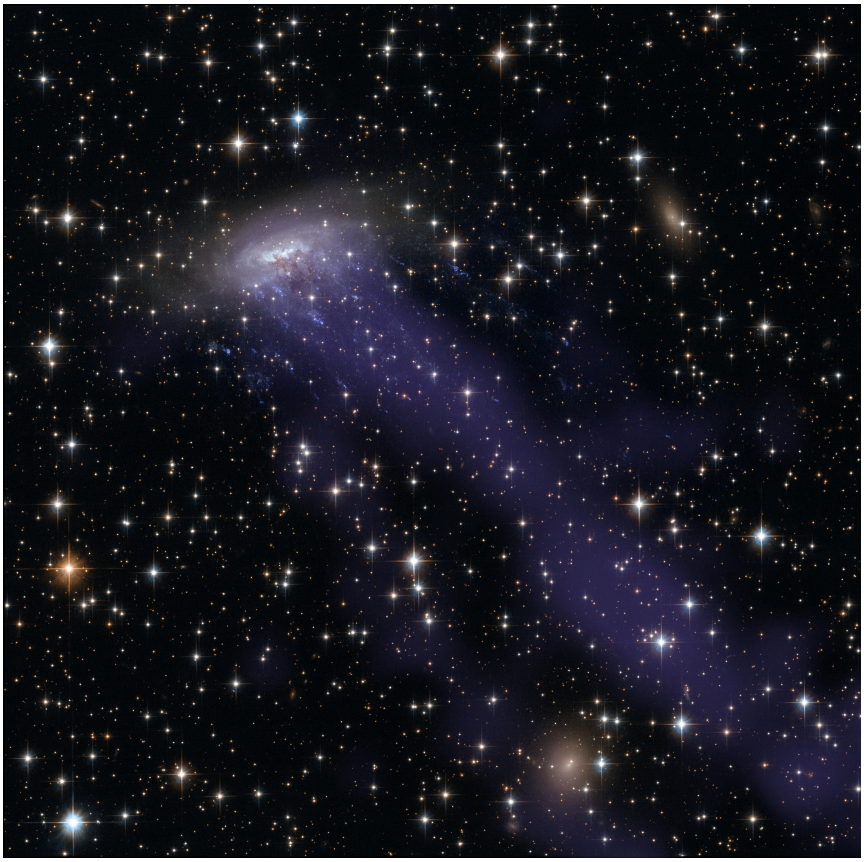

Figure 2.4: ESO 137-001 - a typical jellyfish galaxy. On this image there is a combination of NASA/ESA Hubble Space Telescope observations with Chandra X-ray Observatory. The giant stream of gas extending to the lower right edge is visible only in X-ray. Credit: NASA, ESA, CXC.

RPS tails are detected in various gas phases (ionised, atomic, molecular). They are also detected in dust. New stars can be formed in the tails.

It may be assumed that ISM (material that is stripped from galaxies) stay along the past orbit of galaxy. We will take advantage of this in our following work - from the direction of the galaxy's tail on the sky, we will measure the direction of its velocity components in the plane of the sky.

2.4 Orbits of RPS galaxies in clusters

We assume that jellyfish galaxies, i.e. galaxies currently undergoing active stripping of their ISM, are falling into clusters for the first time. Then, gradually these galaxies lose ISM because of ram pressure.

RPS galaxies provide an additional information about their orbit in comparison to normal galaxies thanks to their tails of stripped ISM. These tails indicate the orbital direction in the plane of sky.

In this work, we will model orbits of jellyfish galaxies observed in the Coma cluster. We will work with fixed and free orbital parameters. Fixed parameters are

the ones we know from observations - the projected location of the galaxy relative to the cluster centre (it is the position on the sky - equatorial coordinates) and the line-of-sight (= radial) velocity component. The free parameters are the line-of-sight distance from the cluster centre plane and the size of the velocity component in the sky plane.

The orbit of a galaxy in the cluster is determined by the gravitational potential of the cluster. The shapes of the orbits can be characterized by the ratio of their apocentric to pericentric distances and their closest approach to the cluster center. Cosmological N-body simulations of satellite halos infalling into clusters (e.g., Wetzel 2011, see also Köppen et al. 2018) indicate that the orbits have mostly an eccentricity of 0.87, which gives a ratio of apocentric to pericentric distance

$$\frac{r_{\mathrm{a}}}{r_{\mathrm{p}}} \approx 14 \tag{2.3}$$

2.5 Our sample galaxies

In this work we will model orbits of two late-type galaxies - NGC 4858 and D100. These are jellyfish galaxies observed in the central parts of the Coma cluster. Due to the interaction with the cluster ICM, they have disturbed disks and extended tails of RPS material. The two galaxies both show bright RPS tails observed in multiple wavelengths (Yagi et al. 2010; Cramer et al. 2019; Roberts and Parker 2020; Jáchym et al. 2017), but with strikingly different morphology. It will be of strong interest to compare their orbits in the Coma cluster and to learn their orbital parameters.

2.5.1 Galaxy NGC 4858

Galaxy NGC 4858 (also known as GMP 3816) is a member of the Coma cluster. It's classification is Barred Spiral (Bb) according to the Hubble and de Vaucouleurs galaxy morphological classification[10] (see Fig. 2.5). NGC 4858 is at a projected distance of about 380 kpc from the center of the Coma cluster. It's stellar mass is $\sim 2.5 \times 10^9\ M_\odot$ (Boselli, Fossati, and Sun 2022). NGC 4858 is a jellyfish spiral galaxy: it is observed to have a one-sided tail of knots of material distributed over the length of at least 30 kpc. These knots originate from the galaxy, extend and tear from the galaxy to add or change the galaxy's structure. Fig. 2.6 shows a HST image of the galaxy and its surroundings. The knots of material extending in the figure upwards from the galaxy are clearly visible [11].

[10] https://theskylive.com/sky/deepsky/ngc4858-object

[11] https://science.nasa.gov/missions/hubble/hubbles-galaxies-with-knots-bursts

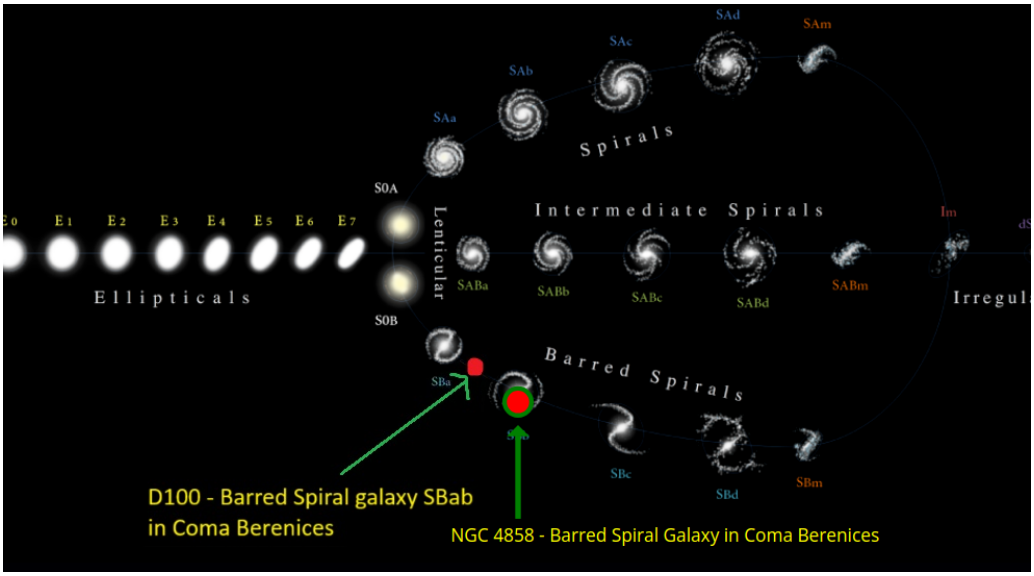

Figure 2.5: Classification of our sample galaxies NGC 4858 and D100, credit: theskylive.com, Antonio Ciccolella

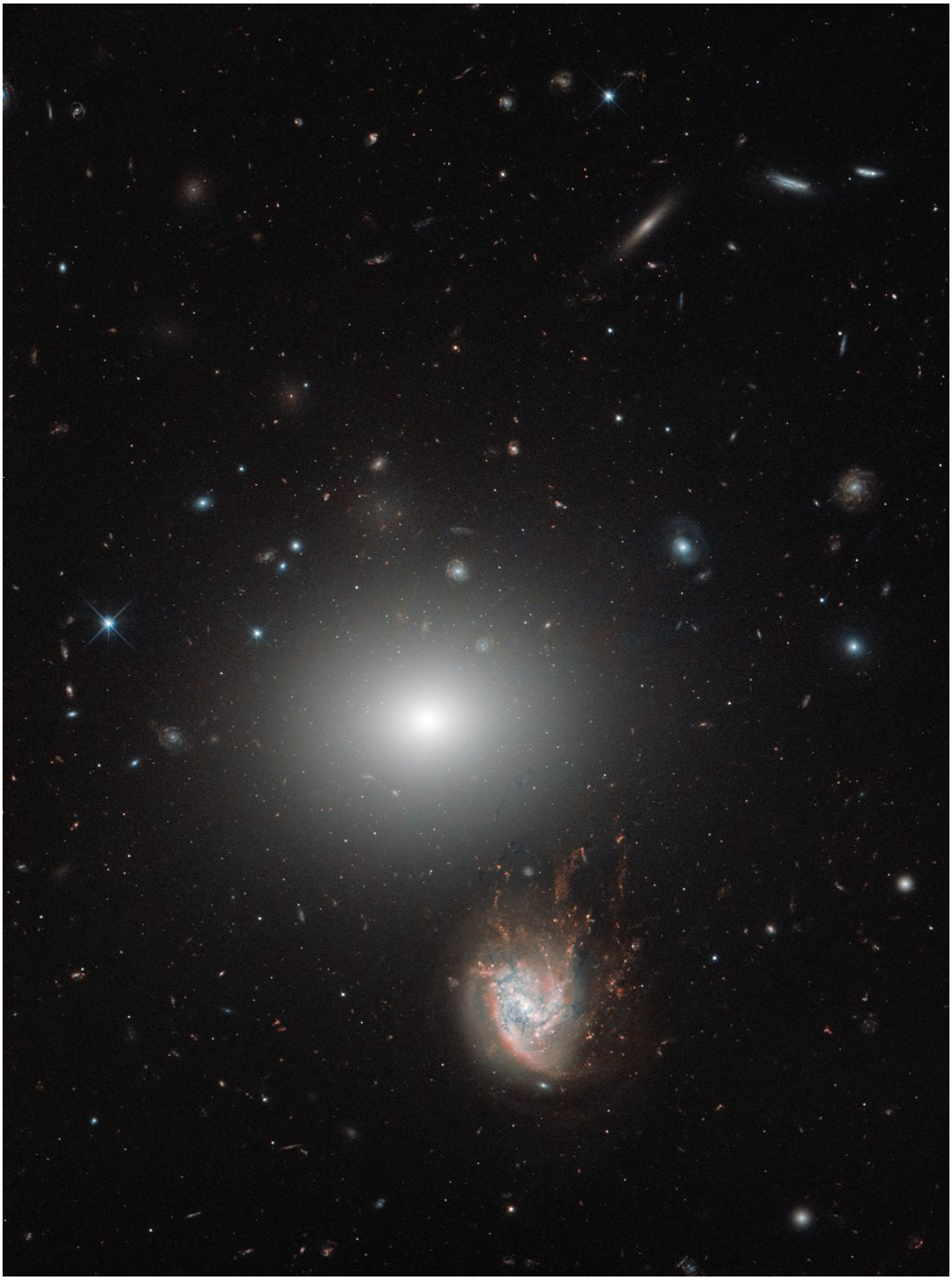

Figure 2.6: The Coma cluster jellyfish galaxy NGC 4858 and its surroundings in an image captured by the Wide Field Camera 3 (WFC3) on HST. NGC 4858 is the disturbed spiral galaxy in the bottom part of the image. The bright centrally-located galaxy is the background elliptical galaxy NGC 4860. Credit: ESA/Hubble and NASA

2.5.2 Galaxy D100

Galaxy D100 (also known as GMP 2910) is another spiral jellyfish galaxy in the Coma cluster. It is classified as SBab (fig. 2.5). It's stellar mass is $\sim 1.8 \times 10^9\ M_\odot$ (Boselli, Fossati, and Sun 2022). D100 is at a projected distance about 240 kpc from the center of the Coma cluster. It has a very straight and narrow, 60 kpc long ram pressure tail, which we can see in a HST view in Fig. 2.7 (Cramer et al. 2019).

Figure 2.7: D100 (the one with the long red tail). A HST image in false colors. The bright red jellyfish tail is Hα data from Subaru Suprime-Cam. Source: Cramer et al. 2019.

2.5.3 Phase - Space diagram

The phase - space diagram (fig. 2.8) is a dependence of the velocity on distance to the cluster center. It shows a journey of a galaxy from field (out of a cluster) into a cluster. A galaxy falling into a cluster does not get trapped into the gravitational potential of the cluster immediately during the first infall. The galaxy flies out from the cluster and then falls into the cluster again. This process repeats several times before the galaxy finally gets trapped in the gravitational potential of the cluster. There is a point called "backsplash". This is a point of the galaxy's orbit when the galaxy flies out from the cluster for the first time[12].

[12] https://astrobites.org/2019/05/23/journey-to-the-centre-of-a-galaxy-cluster/

We will plot our galaxies into this diagram (approximately). Needed values are in table (2.1).

Table 2.1: Values for Phase-Space diagram for galaxies NGC 4858 and D100.

Galaxy	$\frac{V_{\mathrm{LOS}}}{\sigma_{\mathrm{LOS}}}$	$\frac{R_{\mathrm{LOS}}}{R_{200}}$
NGC 4858	2.51	0.19
D100	1.79	0.12

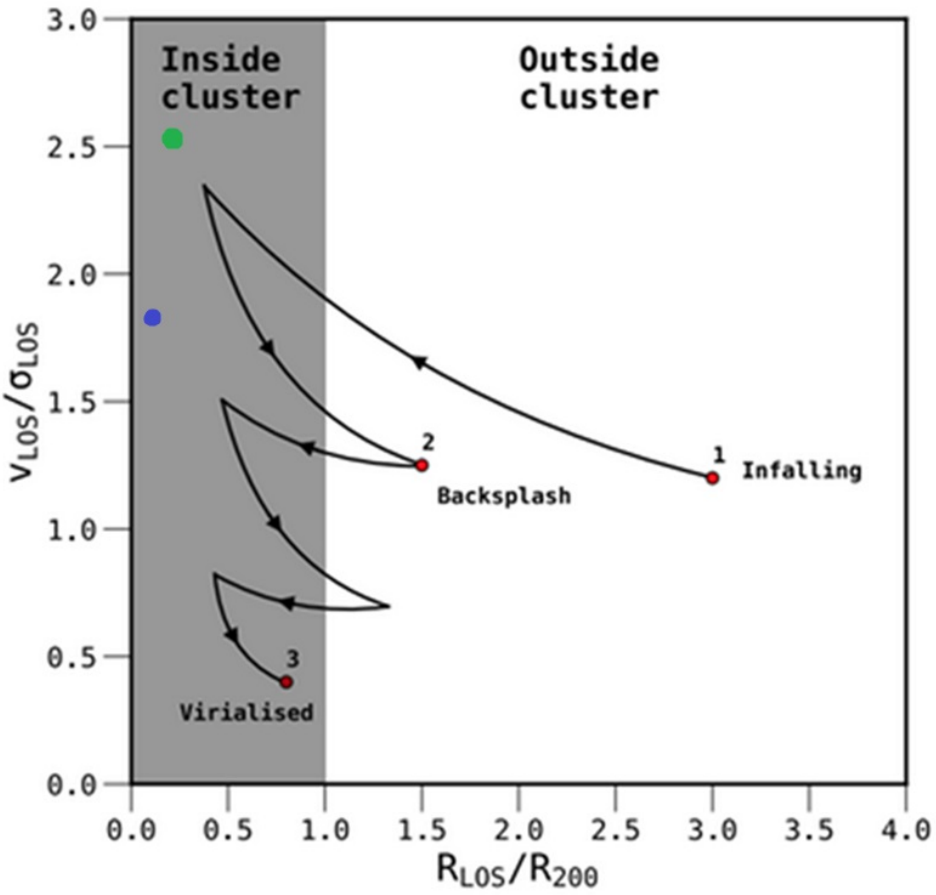

Figure 2.8: Phase-Space diagram showing a journey of an infalling galaxy. R_{200} is a virial radius of a cluster and R_{LOS} is the projected distance on the sky. V_{LOS} is a radial velocity and σ_{LOS} is a velocity dispersion. For Coma cluster $\sigma_{\mathrm{LOS}} = 930\,\mathrm{km\,s^{-1}}$ (Roberts and Parker 2020). The locations of our two galaxies are marked: NGC 4858 (green) and D100 (blue). Source: Astrobites

Chapter 3

Methods

In order to explore the orbital history of the two galaxies in the Coma cluster, we will numerically integrate their motion in the cluster. For the numerical integration of the equation of motion of the galaxies (represented as test particles), we will use the Runge-Kutta method (described in 3.1.1). The gravitational potential of the cluster will be modeled with a Navarro-Frenk-White profile introduced in 3.2.1. To evaluate the ram pressure stripping history of the galaxies, we will model the distribution of the ICM in the cluster with a β-model introduced in 3.2.2.

3.1 Numerical integrations

To simulate the evolution of dynamical systems (which are described by differential equations), a number of various numerical methods can be used. Following e.g., the online course on dynamical systems[1], we can consider a simple system described by this equation:

$$\dot{x} = f(t, x) \tag{3.1}$$

with an initial condition:

$$x(t_0) = x_0 \tag{3.2}$$

The solution of this system is a trajecotory $x = x(\mathrm{t})$. Most of the practical problems do not have an analytical solution so we have to find a trajectory by a numerical method. The basic idea of a numerical solution is to make the variables discrete. This means that instead of a continuous trajectory (the analytical solution) we use a sequence of discrete points $x_0(t_0), x_1(t_1)$,... The independent variable is time t. Values of the variable t make so-called knots of the net. If the points are dense enough they make an approximate representation of the orbit. The distance between two neighbouring points of the net is

$$h_\mathrm{i} = t_{\mathrm{i}+1} - t_\mathrm{i} \tag{3.3}$$

[1] https://www.fce.vutbr.cz/aiu/macur.j/Dynsys/kap7/kap7.htm

and it is called the step of the method (in general it does not have to be constant, but for us it will be always a constant).

We always calculate the new state of the system in the time t_{i} on the basis of the previous states $t_{\mathrm{i-k}}$. If k is 1 we call it one-step method. In one-step method we calculate the new state from the previous state. The easiest one-step method is the Euler's method. The equation for this method is

$$x_{\mathrm{n+1}} = x_{\mathrm{n}} + h \cdot f(t_{\mathrm{n}}, x_{\mathrm{n}}). \tag{3.4}$$

Equation (3.4) can be derived for example from the Taylor series in the surroundings of point $x_{\mathrm{n}} = x(t_{\mathrm{n}})$. After adjustment, it leads to equation

$$x_{\mathrm{n+1}} = x_{\mathrm{n}} + h \cdot f(t_{\mathrm{n}}, x_{\mathrm{n}}) + \frac{h^2}{2} \cdot \dot{f}(t_n, x_n) + ... \tag{3.5}$$

so we see that the Euler's formula is a linear approximation of the Taylor series.

In praxis we can not use the Euler's method. The new state calculated by us responds to reality only if the velocity of the system is constant. This method is not enough accurate.

3.1.1 The numerical method Runge - Kutta

Runge - Kutta method can be also derived from the Taylor series. It counts with the members of the higher orders. There are more Runge - Kutta methods, the most favourite is the classical method of the fourth order. The new state of the system is calculated with these relations

$$\begin{aligned} k_1 &= f(t_n, x_n) \\ k_2 &= f(t_n + \frac{h}{2}, x_n + k_1 \cdot \frac{h}{2}) \\ k_3 &= f(t_n + \frac{h}{2}, x_n + k_2 \cdot \frac{h}{2}) \\ k_4 &= f(t_n + h, x_n + k_3 \cdot h) \\ x_{n+1} &= x_n + \frac{h}{6} \cdot (k_1 + 2k_2 + 2k_3 + k_4). \end{aligned} \tag{3.6}$$

The values k_i represent velocities (the derivations of state) in distinguished points in the beginning, in the middle and at the end of the interval $\langle t_n, t_{n+1} \rangle$.

3.2 Navarro-Frenk-White profile and ICM in clusters

3.2.1 Navarro-Frenk-White profile

The Navarro-Frenk-White (NFW) profile is one of the most used profiles describing the distribution of dark matter in galaxies and clusters (Brilenko, Eingorn, and Zhuk 2017). The equation for the dark matter distribution is

$$\rho(r) = \frac{\delta_c \rho_c}{\frac{r}{r_s}(1+\frac{r}{r_s})^2} \tag{3.7}$$

which is actually the density of dark matter as a function of distance from the cluster center. δ_c is the halo overdensity and r_s is the scale radius.

Mass of the cluster is given by integral

$$M = \int_0^r 4\pi r^2 \rho(r)\, dr. \tag{3.8}$$

From equation (3.8) we get the mass for cluster

$$M = 4\pi\rho_c r_s^3 \left[\ln\left(1+\frac{r}{r_s}\right) - \left(\frac{r}{r_s+r}\right)\right]. \tag{3.9}$$

ρ_c is the critical density at the redshift of the cluster and may be expressed as

$$\rho_c = \frac{3H^2}{8\pi G}, \tag{3.10}$$

where H is Hubble constant and G is gravitational constant. δ_c is the halo overdensity and can be written as

$$\delta_c = \frac{200}{3}\frac{c^3}{\ln(1+c) - \frac{c}{1+c}}, \tag{3.11}$$

where c is the halo concentration, and r_s is defined as

$$r_s = \frac{r_{200}}{c}, \tag{3.12}$$

where r_{200} is the virial radius, i.e., the radius within which the mean density is 200 times the critical density of the Universe [2].

We will model the gravitational potential of the Coma cluster with a NFW profile with the parameters in table 3.1.

3.2.2 Distribution of ICM in clusters

Density of the ICM as a function of distance from the cluster center is modeled with a β-profile

$$\rho_{\mathrm{ICM}}(r) = \rho_0 \left[1 + \left(\frac{r}{r_c}\right)^2\right]^{-\frac{3}{2}\beta}, \tag{3.13}$$

where ρ_0 is the central ICM density, r_c is the scale-length parameter, and β is the slope parameter. To model the ICM distribution in the Coma cluster, we use the parameters in table 3.1.

[2] https://ned.ipac.caltech.edu/level5/March15/Roos/Roos3.html

Table 3.1: Values of quantities for Coma cluster (Kubo et al. 2007, Fossati et al. 2012)

Quantity	Value	Unit
ρ_0	$6,3 \cdot 10^{-30}$	$\mathrm{kg\,m^{-3}}$
r_c	0,26	Mpc
β	0,7	-
c	3,84	-
r_{200}	1,99	Mpc

3.3 Initial conditions

We will calculate a series of cluster orbits consistent with the observed orbital components of the galaxies NGC 4858 and D100. Using a Python script, we numerically integrate the orbital motion of test particles representing the two galaxies in the gravitational potential of the Coma cluster given by the NFW profile.

For the two galaxies we know from observations their radial (line-of-sight) velocity and their position on the sky (coordinates). Thanks to the presence of jellyfish "tails" in both galaxies, we can assume their direction of motion on the sky. These three orbital parameters are thus fixed from observations: the galaxy current position on the sky, the LOS velocity, and the plane of the sky velocity direction (indicated by the projected tail direction). The free parameters not known from observations are the size of the velocity component on sky and the distance in a radial (line-of-sight) direction.

We take the values of the fixed parameters for the galaxies from the SIMBAD astonomical database[3] and for the Coma cluster from the NASA/IPAC Extragalactic Database (NED)[4]. Table 3.2 summarizes the coordinates of the two galaxies and the Coma cluster center. The location of the center of the cluster corresponds to a position between the two central giant elliptical galaxies NGC 4889 and NGC 4874 which are visible in Fig. 2.2.

Table 3.2: Coordinates of galaxies NGC 4858 and D100 and Coma cluster centre.

object	RA	Dec	radial velocity $[\mathrm{km\,s^{-1}}]$
Coma cluster	$12^h59^m48.7329^s$	$27°58'50.499''$	6933
NGC 4858	$12^h59^m2.072^s$	$28°6'56,23''$	2336
D 100	$13^h00^m9.141^s$	$27°51'59.34''$	-1665

We used the astronomical imaging and data visualization application SAOImage DS9[5] to measure the current location of the galaxies in the Coma cluster, which will serve as initial conditions in our modeling. Using FITS images of our galaxies and coordinates of the center of the Coma cluster we measured angular distances in X

[3] https://simbad.u-strasbg.fr/simbad
[4] http://ned.ipac.caltech.edu
[5] https://sites.google.com/cfa.harvard.edu/saoimageds9

and Y axis (RA, Dec). Fig. 3.1 illustrates the measurement of the angular distance of D100 from the cluster center and components of the velocity in the plane of sky in DS9. To recalculate the distances to physical units (megaparsecs), we used the relation $1'' \cong 0.473$ kpc, which corresponds to the Coma cluster distance of 97.5 Mpc (Zadorozhna et al. 2023).

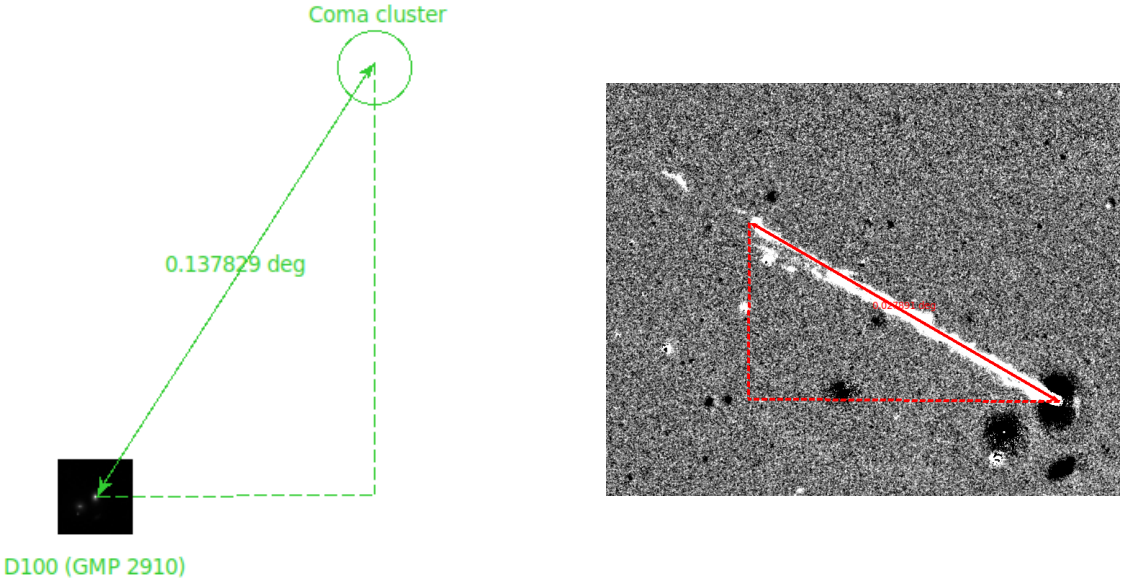

Figure 3.1: Measuring in SAOImage DS9. Measuring angular distances relative to the cluster center (left), velocity components X (the horizontal line) and Y (the vertical line) in the plane of sky (right). Sources: DESI Legacy Survey, optical band (left), Yagi et al. 2010 (right).

This gave us initial conditions x_0 and y_0 - projected location relative to the cluster centre and X and Y components of the direction of RPS tail that gave us inital conditions $v_{\mathrm{x},0}$ and $v_{\mathrm{y},0}$. The RPS tail of NGC 4858 is on the sky oriented vertically (see fig. 3.2), in the S-N direction, we will thus assume the direction of the velocity component on the sky is $-v_{\mathrm{y},0}$ and $v_{\mathrm{x},0} = 0$.

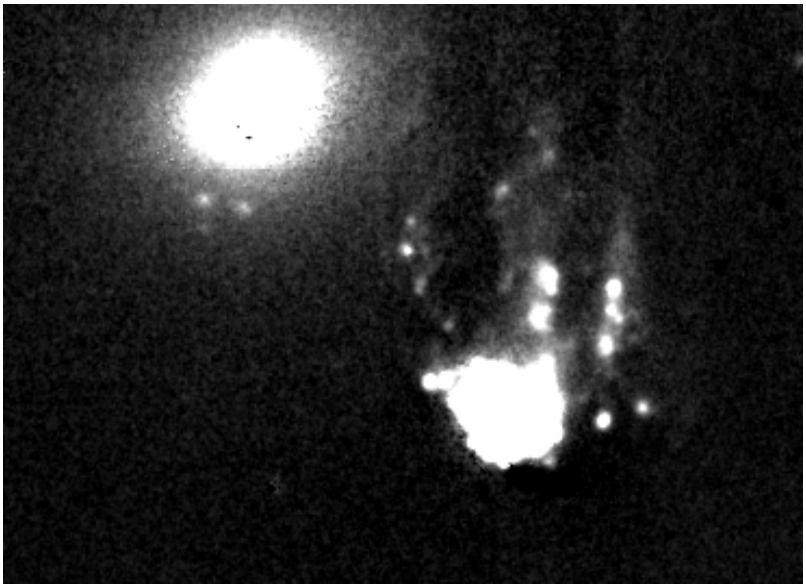

Figure 3.2: Galaxy NGC 4858 with Hα tail. Source: Yagi et al. 2010.

Finally, we calculated the radial velocity relative to the cluster. These calculations gave us the initial conditions that we will use in the modelling of orbits of the galaxies. The measured fixed initial conditions for both galaxies are summarized in Table 3.3.

Table 3.3: Measured fixed parameters for our galaxies.

Galaxy	x_0 [kpc]	y_0 [kpc]	$v_{x,0}$ [km s^{-1}]	$v_{y,0}$ [km s^{-1}]	$v_{z,0}$ [km s^{-1}]
NGC 4858	293	228	$0 \cdot V$	$-1 \cdot V$	2336
D100	-127	-194	$0.869 \cdot V$	$0.496 \cdot V$	-1665

Table 3.4: Free parameters for galaxy NGC 4858.

z_0 [kpc]	V_{xy} [km s^{-1}]	V_{xy} [km s^{-1}]	V_{xy} [km s^{-1}]	V_{xy} [km s^{-1}]
-500	500	1167	1833	2500
-250	500	1167	1833	2500
0	500	1167	1833	2500
250	500	1167	1833	2500
500	500	1167	1833	2500

Table 3.5: Free parameters for galaxy D100.

z_0 [kpc]	V_{xy} [km s^{-1}]	V_{xy} [km s^{-1}]	V_{xy} [km s^{-1}]	V_{xy} [km s^{-1}]	V_{xy} [km s^{-1}]	V_{xy} [km s^{-1}]
−500	500	1100	1700	2300	2900	3500
−250	500	1100	1700	2300	2900	3500
0	500	1100	1700	2300	2900	3500
250	500	1100	1700	2300	2900	3500
500	500	1100	1700	2300	2900	3500

The modelling is based on exploring a wide range of values of free parameters. This will provide us with a wide range of possible orbits. We will analyze the orbits and try to determine the parameters of the most probable orbits. For the free parameters: Line-of-sight distance from the cluster centre plane (z_0) and size of the velocity component in the plane of sky (V_{xy}), we use for both galaxies the following range of z_0, from -0.5 Mpc to 0.5 Mpc, specifically z_0 = -0.5 Mpc, -0.25 Mpc, 0 Mpc, 0.25 Mpc and 0.5 Mpc. For each of these z_0, we modeled four values of V_{xy} for NGC 4858, from $0.5 \cdot 10^3$ km s^{-1} to $2.5 \cdot 10^3$ km s^{-1}, which correspond to the deprojected velocity V = 500 km s^{-1}, 1167 km s^{-1}, 1833 km s^{-1} and 2500 km s^{-1}, and for D100, we modelled six values of V from $0.5 \cdot 10^3$ km s^{-1} to $3.5 \cdot 10^3$ km s^{-1}, which correspond to V = 500 km s^{-1}, 1100 km s^{-1}, 1700 km s^{-1}, 2300 km s^{-1}, 2900 km s^{-1} and 3500 km s^{-1} . The ranges of the free parameters are summarized in table 3.4 for NGC 4858 and in table 3.5 for D100.

Chapter 4

Results

The main goal of our work is to study and analyze the orbits of the jellyfish galaxies NGC 4858 and D100 in the Coma cluster. Using the initial conditions introduced in the previous section, we vary the free parameters in order to model 20 orbits for each galaxy. These orbits are all consistent with the current observed fixed parameters. In order to follow the orbits to both directions from the initial location, we run two executions of the model, one with positive, and another with negative time step. We plot the projections of the orbits, follow the evolution of the distance of the galaxies from the cluster center, their total orbital velocity, as well as the evolution of the ram pressure that the galaxies experience along the orbits. We aim to describe the principal parameters of the orbits, such as the pericentric distance, time to/from pericenter, learn about the ram pressure history along the orbits, and based on ad-hoc assumptions and comparison with orbital statistics resulting from cosmological simulations, we attempt to constrain the range of suitable orbits. We first present the results for NGC4858 in Section 4.1, and then for D100 in Section 4.2.

4.1 Galaxy NGC 4858

The model orbits are presented in series of Figures corresponding to different initial values of the free parameter z_0. Each figure contains four different orbits corresponding to different initial values of the second free parameter, the velocity component V.

Figure 4.1 corresponds to $z_0 = -500$ kpc, i.e., the galaxy is initially located 500 kpc closer to us than the plane containing the center of the cluster. Four different colors correspond to different values of V (curves from blue to red; see the legend giving the corresponding current total 3D velocity).

The top row of Figure 4.1 shows three perpendicular projections of the orbits: RA-Dec, RA-LOS, LOS-Dec (The RA-Dec projection corresponds to the view on the plane of the sky. We use megaparces as units, because it is better to imagine motion of a galaxy in cluster). The initial location of the galaxy is marked with a red cross. The yellow circle indicates the Coma virial radius $r_{200} = 1.99$ Mpc.

The bottom row shows the evolution of ram pressure (left panel), total (i.e., deprojected) cluster-centric distance (middle panel), and total orbital velocity (right

panel). Time $T = 0$ corresponds to the current (initial) location of the galaxy. The orbits were modeled for 3 Gyr (from -1.5 to 1.5 Gyr).

The results corresponding to $z_0 = -250, 0, 250, 500$ kpc are shown in Figs. 4.2, 4.3, 4.4, 4.5.

Figure 4.6 shows the evolution of the deprojected radial distance in units of the pericenter distance for all z_0.

Figure 4.7 shows dependence of peak of ram pressure on distance z_0. We made it from figures 4.1 - 4.5 so that we can better present this dependence in one graph for all initial z_0.

Figure 4.8 shows dependence of pericentric to apocentric ratio on initial line-of-sight distance z_0. We made it from figures 4.6 so that we can better present this dependence in one graph for all initial z_0.

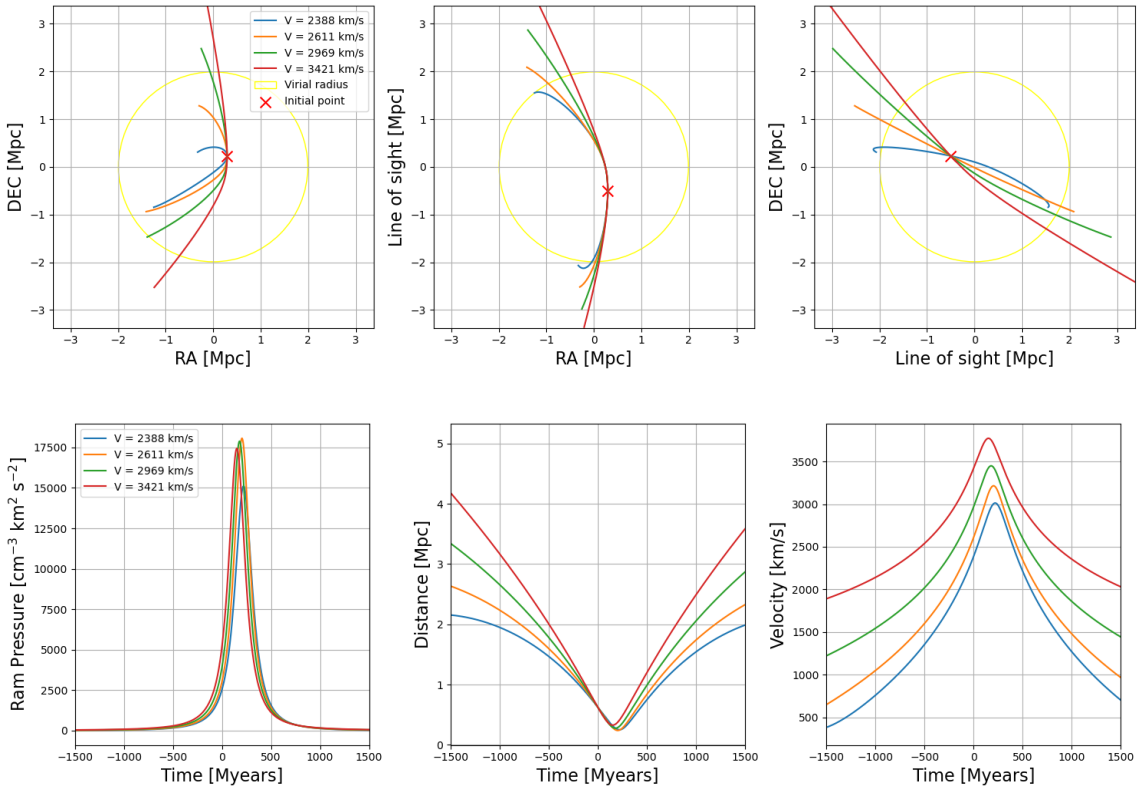

Figure 4.1: NGC 4858: model orbits for $z_0 = -0.5$ Mpc and V in the range from 500 to 2500 km s^{-1} (curves from blue to red). Top row: views of the orbits in RA-Dec, RA-LOS, LOS-Dec projections. Positions of the galaxy in $T = 0$ Gyr are marked with red cross. The virial radius is marked with the yellow circle. The legend gives the total velocities in $T = 0$ Gyr. Bottom row: time dependencies of the ram pressure (left), deprojected distance from the cluster center (middle) and deprojected velocity (right).

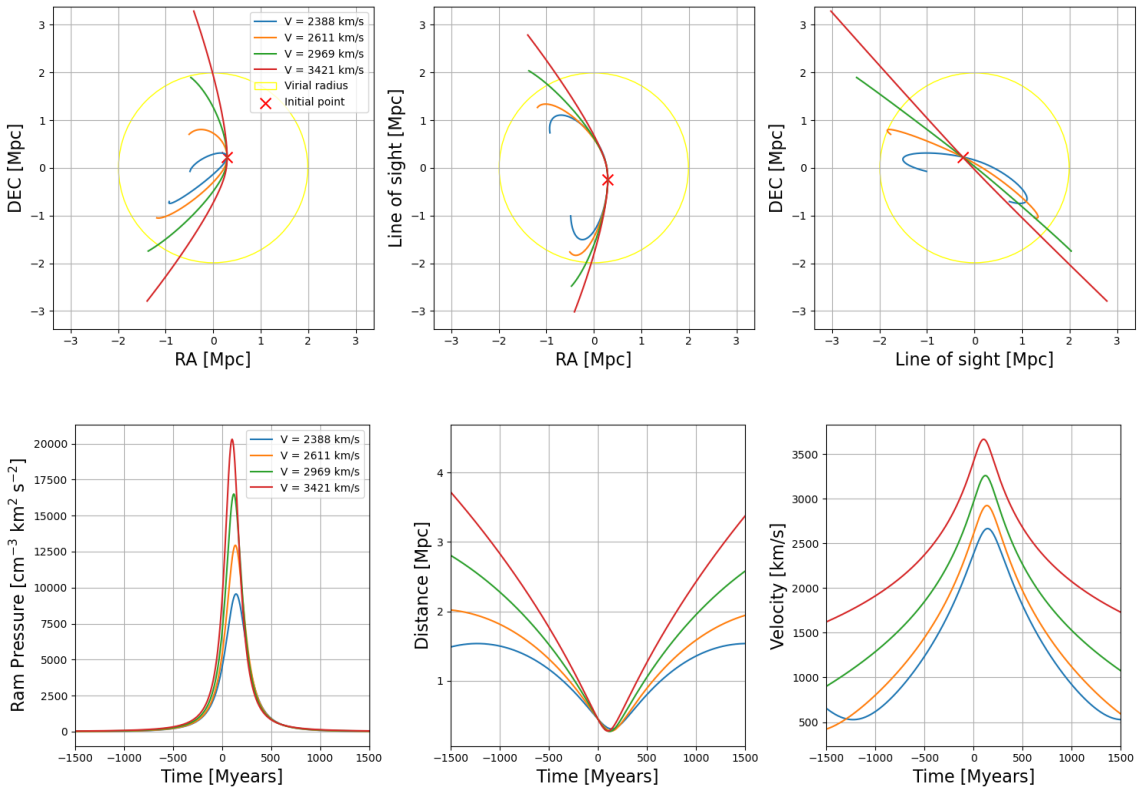

Figure 4.2: The same as in Fig. 4.1, but for $z_0 = -0.25$ Mpc

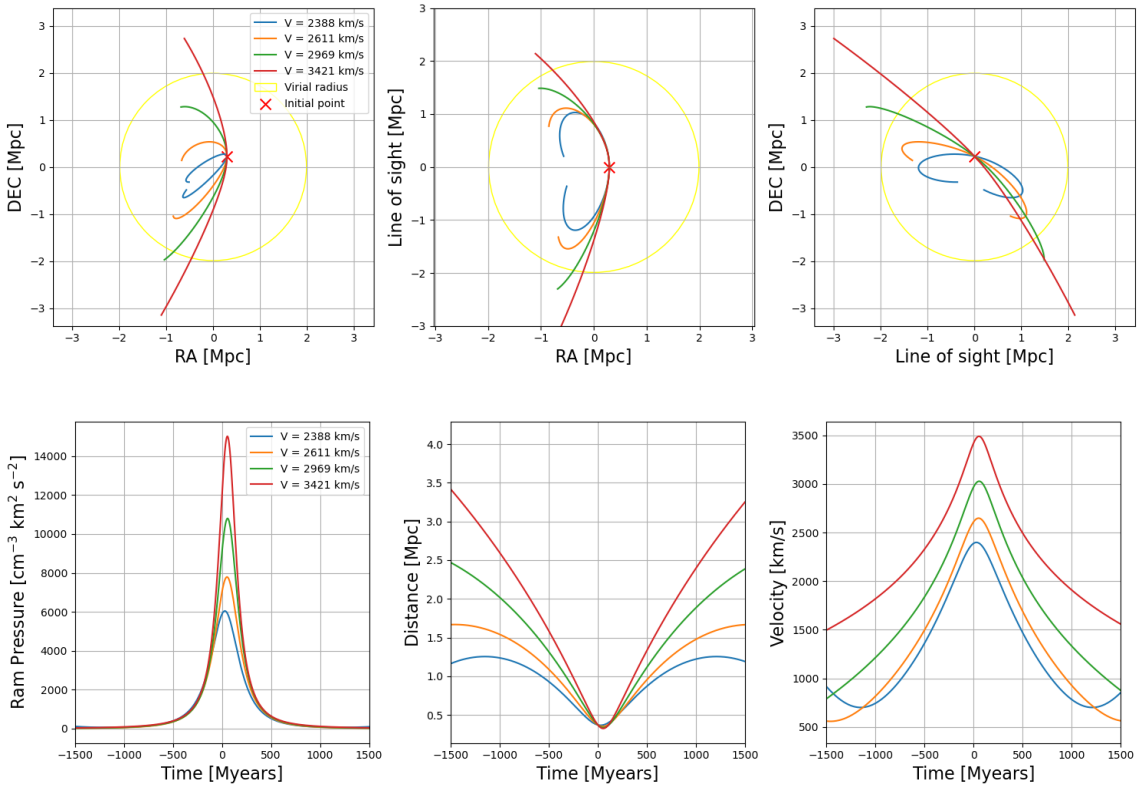

Figure 4.3: The same as in Fig. 4.1, but for $z_0 = 0$ Mpc.

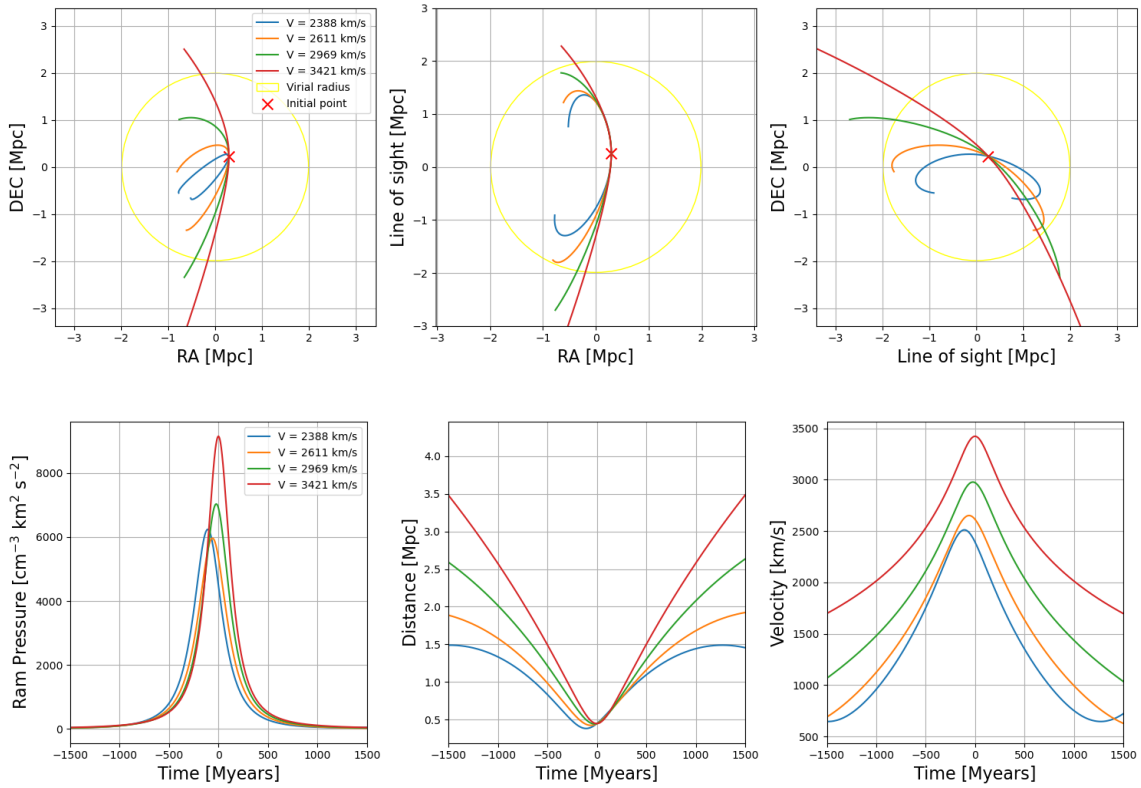

Figure 4.4: The same as in Fig. 4.1, but for $z_0 = 0.25$ Mpc.

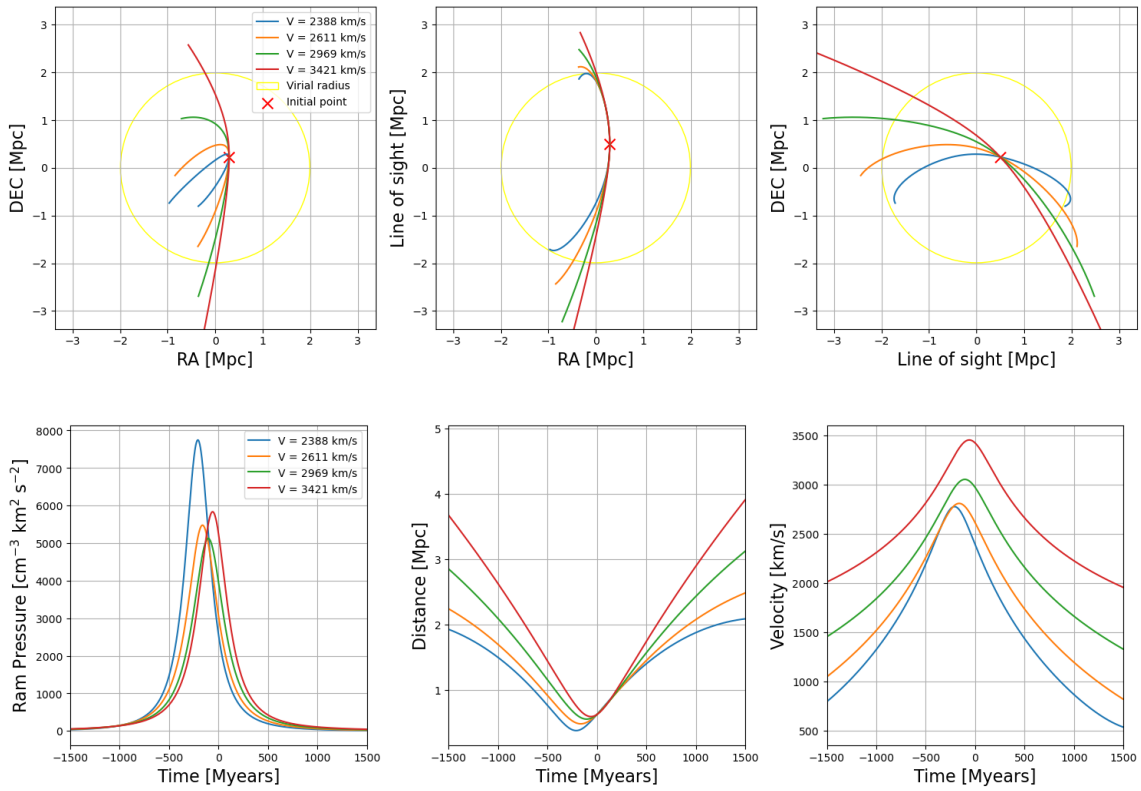

Figure 4.5: The same as in Fig. 4.1, but for $z_0 = 0.5$ Mpc.

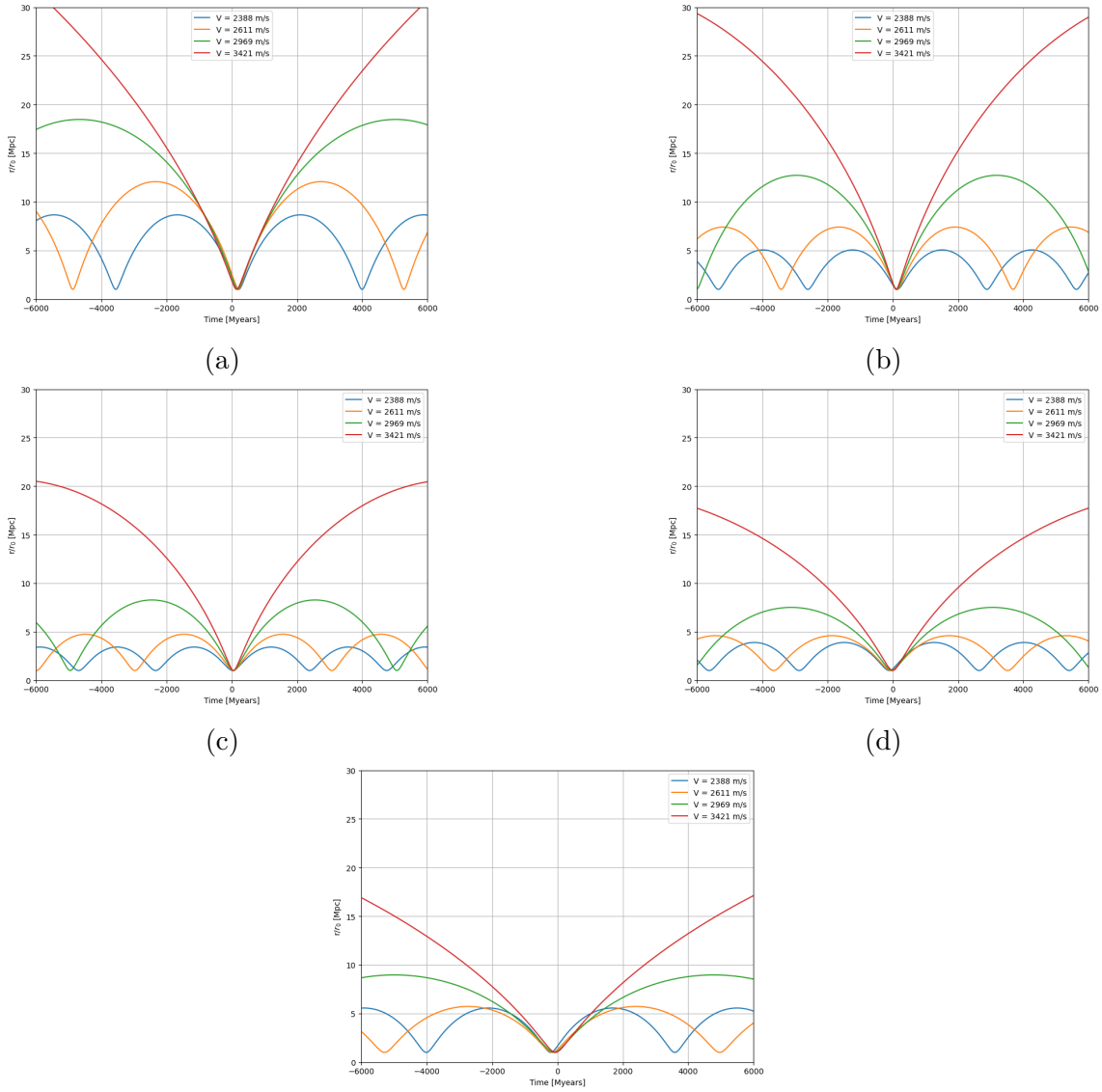

Figure 4.6: NGC 4858: the evolution of the deprojected radial distance in units of the pericenter distance for orbits with z_0 = (a) - 0.5 Mpc, (b) -0.25 Mpc, (c) 0 Mpc, (d) 0.25 Mpc, (e) 0.5 Mpc.

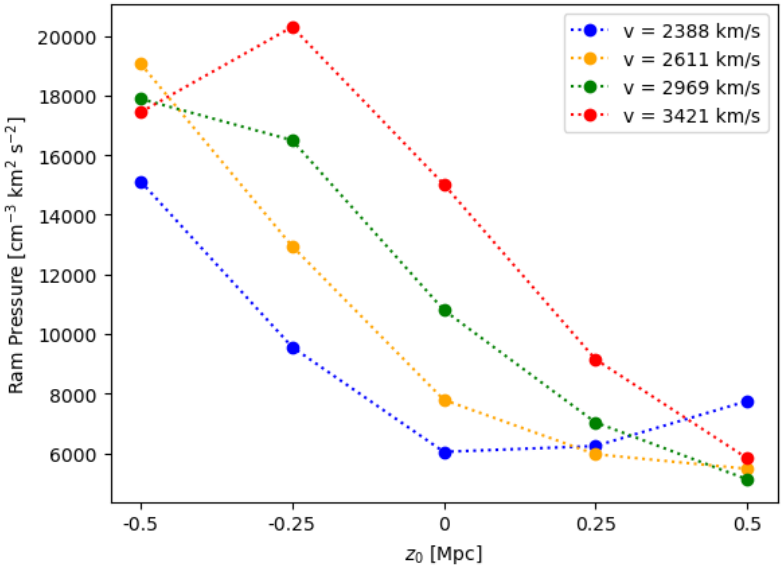

Figure 4.7: Dependence of peak of ram pressure on distance z_0 for various velocities for NGC 4858

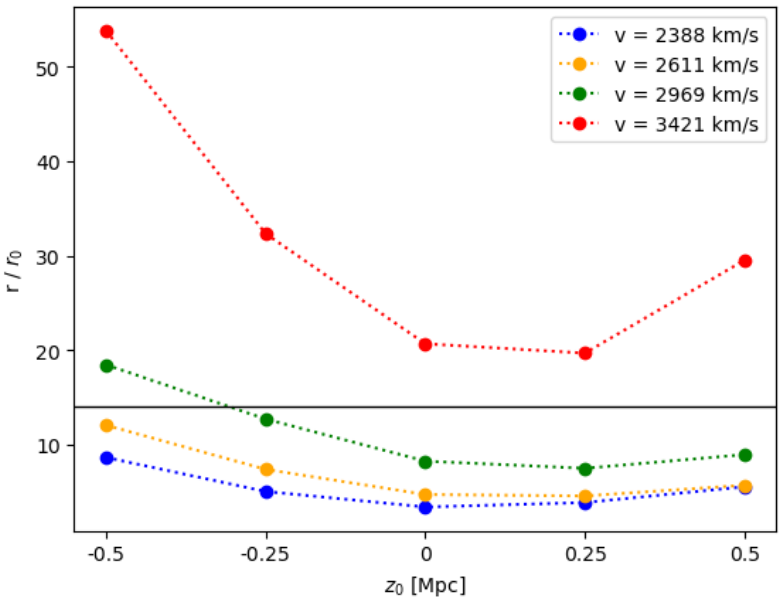

Figure 4.8: NGC 4858: dependence of pericentric to apocentric ratio on intial line-of-sight distance z_0. The horizontal line shows value 14.

From comparison of the model orbits of galaxy NGC 4858 presented in Figures 4.1 - 4.6 we can observe the following trends:

- For orbits with positive values of the initial parameter z_0 (i.e., currently farther away from us than the cluster center), pericenter occurs sooner (it means before $T = 0$ Myear), while for orbits with negative z_0, pericenter occurs later (after

$T = 0$ Myear). The galaxy is currently at pericenter for $z_0 \sim 100$ kpc (not shown).

- The pericenter distances of the model orbits are in the range of about 0.3 - 0.5 Mpc, while the times from/to pericenter are in the range 0 - 200 Myr.

- Smaller velocities (i.e., low deprojected velocity V) result in more compact orbits (i.e. orbits not crossing virial radius), larger velocities in more elongated ones. The slowest orbits ($V = 2400$ - $2600\,\mathrm{km\,s^{-1}}$) in most cases do not cross the virial radius of the cluster, while the fastest orbit ($V = 3400\,\mathrm{km\,s^{-1}}$) might be too elongated, only marginally bound to the cluster.

- Peak of the ram pressure along the orbits with negative z_0 is considerably higher than for orbits with positive z_0. Thus, if NGC 4858 is at an orbit with negative z_0, it will experience in the near future ($\sim$ 250 Myr) a steep increase of ram pressure. If, on the contrary, it is at a positive z_0 orbit, it has already experienced the peak of ram pressure, which moreover was much weaker. This behavior is well visible in Fig. 4.7 which plots the peak of ram pressure as a function of z0. For $z_0 = -500$ kpc, the peak values reach $15,000 - 20,000$ $\mathrm{cm^{-3}\,km^2\,s^{-2}}$, while for $z_0 = 500$ kpc, only about $5,000 - 8,000$ $\mathrm{cm^{-3}\,km^2\,s^{-2}}$.

- The shape of the orbits can be described by the ratio of its apocenter to pericenter distances and its closest approach to the centre. Fig. 4.8 summarizes the values of the ratio for orbits with different z_0's and initial velocities. In cosmological N-body simulations (Köppen et al. 2018), the orbits of infalling galaxies have mostly a ratio $r_{\mathrm{apo}}/r_{\mathrm{peri}}$ about 14. The plot in Fig. 4.8 shows that the fastest modeled orbit (V = $3400\,\mathrm{km\,s^{-1}}$) has the ratio too high (except a range of z_0 from 0 to 250 kpc). For the other three velocities, the ratio is good for negative z_0. Fig. 4.8 also shows a trend - for all velocities, the ratio decreases from negative z_0 towards positive z_0. It begins to grow again approximately at $z_0 = 0.25$ Mpc. This trend is very distinct for highest velocity.

- From modeled orbits we can specify that the lower limit of possible velocities is about $V = 3000\,\mathrm{km\,s^{-1}}$. From the apocenter to pericenter ratio we can say that the top limit of possible velocities is for a velocity a little higher than $3400\,\mathrm{km\,s^{-1}}$, because for this velocity the ratio is too high for most of the z_0 except of a range 0 - 250 kpc. We can also say that for velocity $3400\,\mathrm{km\,s^{-1}}$, the probable values of z_0 are 0 - 250 kpc. For velocities lower than $3400\,\mathrm{km\,s^{-1}}$, probable values of z_0 are the negative ones. The most probable orbit is the one with $V = 3000\,\mathrm{km\,s^{-1}}$ for the negative z_0.

4.2 Galaxy D100

Following figures show the same as in 4.1, but Figures for each z_0 show six orbits. All following Figures are for galaxy D100.

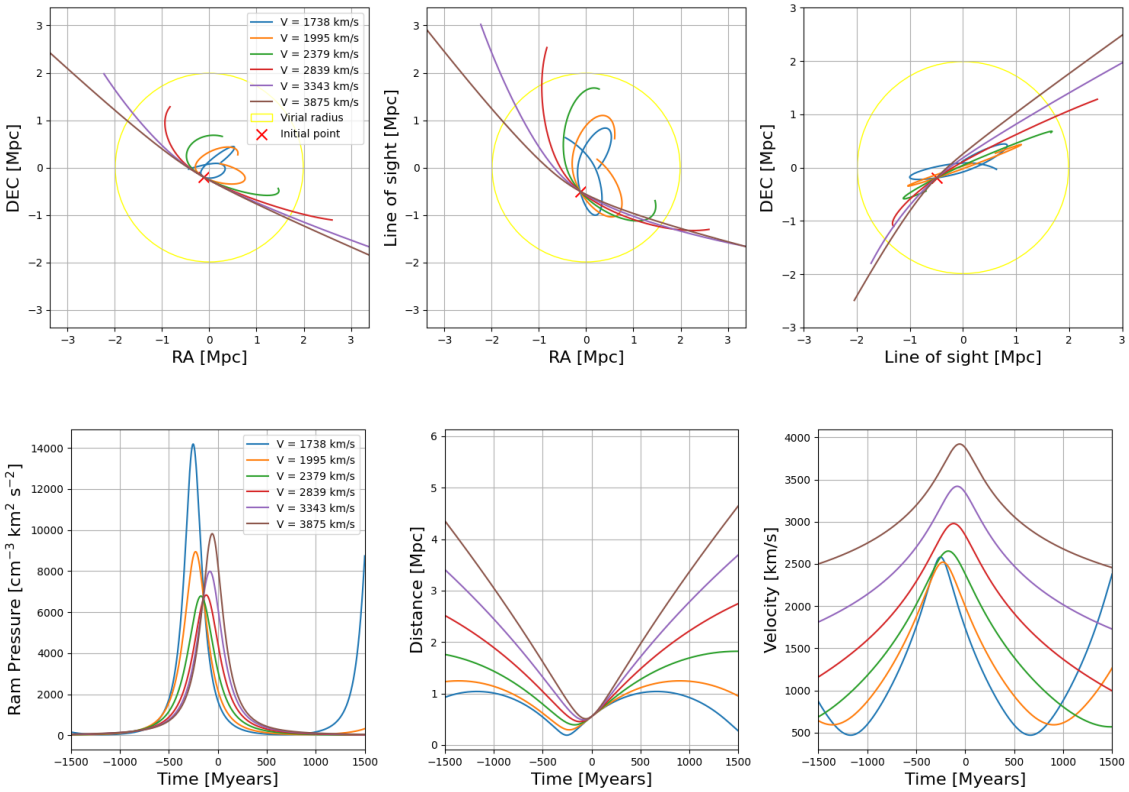

Figure 4.9: D100: model orbits for $z_0 = -0.5$ Mpc and V in the range from 1700 to 3900 km s^{-1} (curves from blue to brown). Top row: views of the orbits in RA-Dec, RA-LOS, LOS-Dec projections. Positions of the galaxy in $T = 0$ Gyr are marked with red cross. The virial radius is marked with the yellow circle. The legend gives the total velocities in $T = 0$ Gyr. Bottom row: time dependencies of the ram pressure (left), deprojected distance from the cluster center (middle) and deprojected velocity (right).

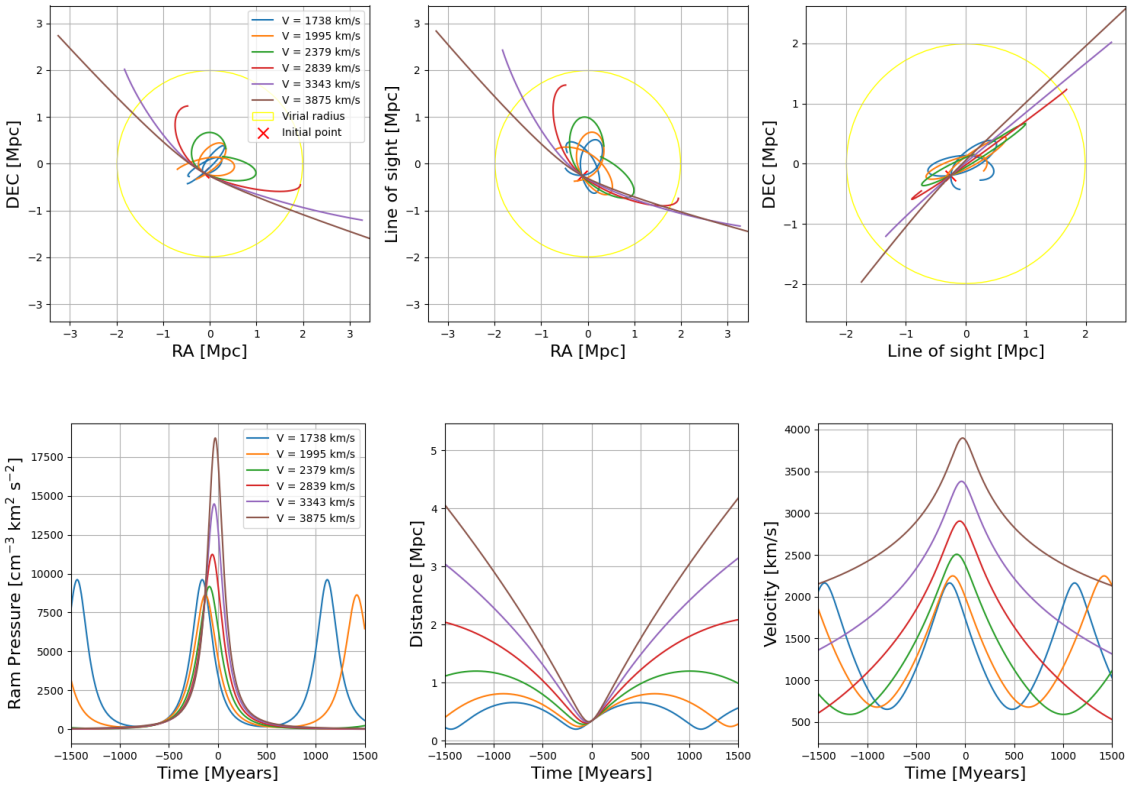

Figure 4.10: The same as in Fig. 4.9, but for $z_0 = -0.25$ Mpc

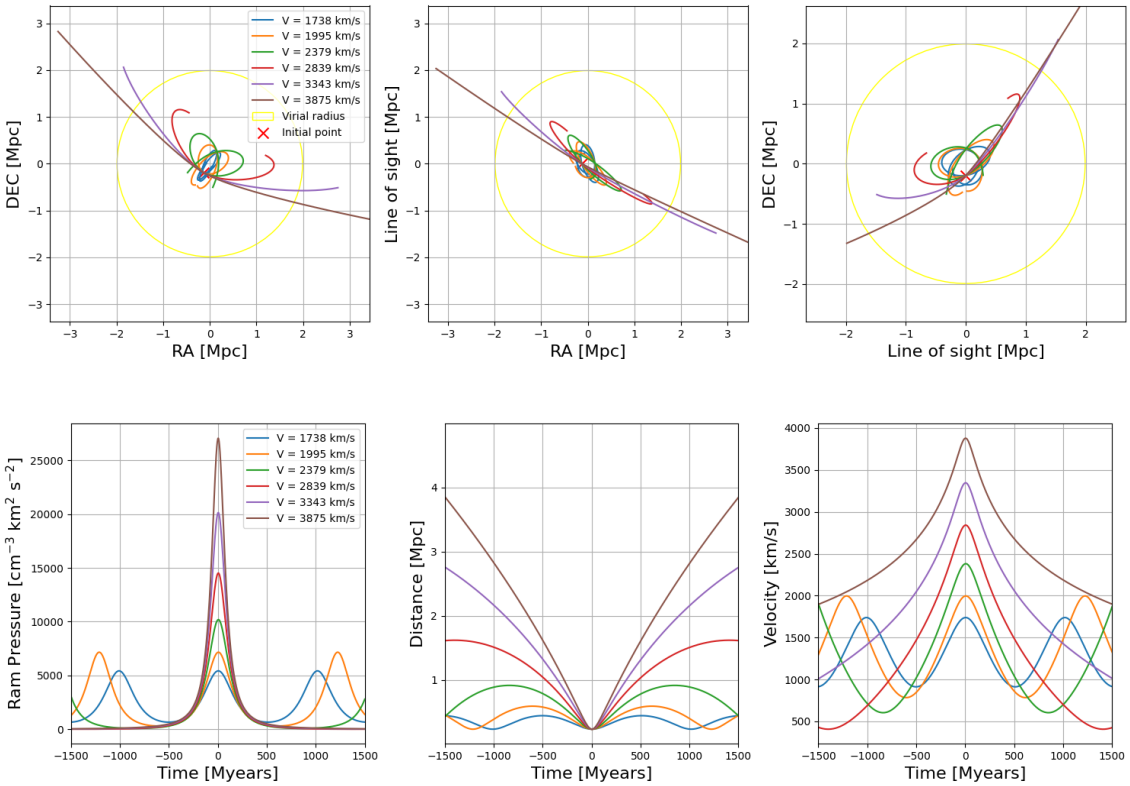

Figure 4.11: The same as in Fig. 4.9, but for $z_0 = 0$ Mpc

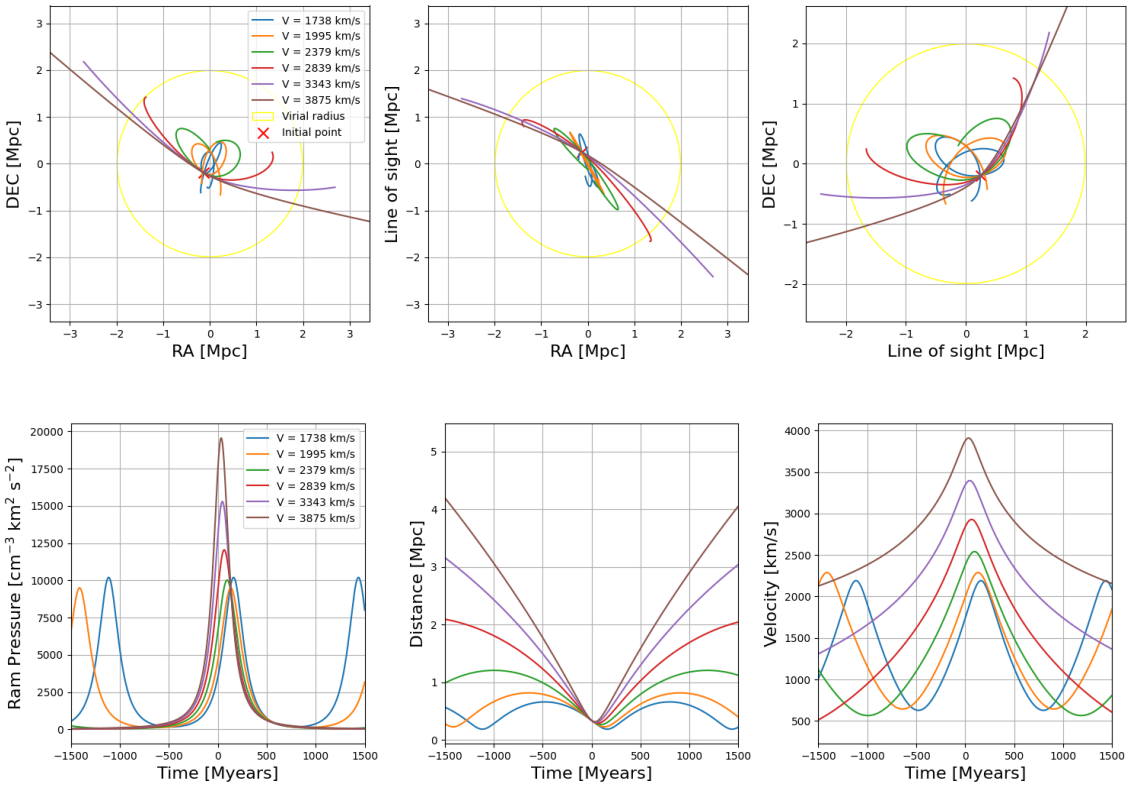

Figure 4.12: The same as in Fig. 4.9, but for $z_0 = 0.25$ Mpc

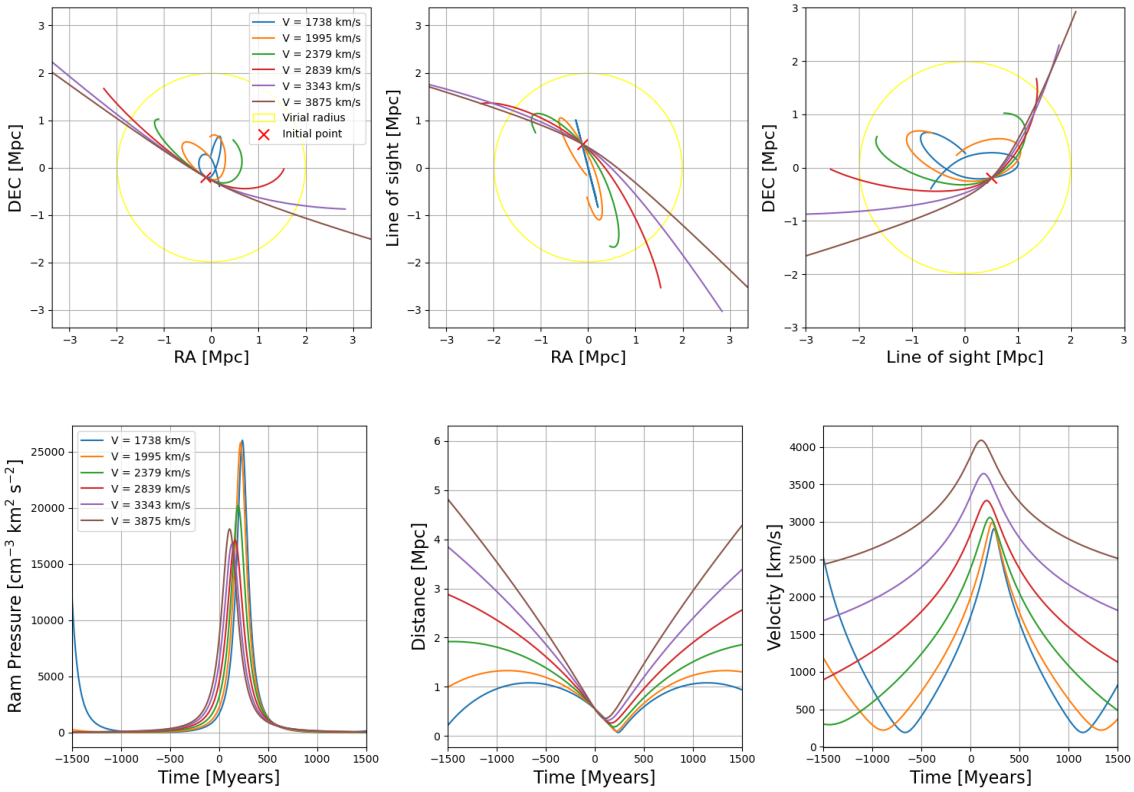

Figure 4.13: The same as in Fig. 4.9, but for $z_0 = 0.5$ Mpc

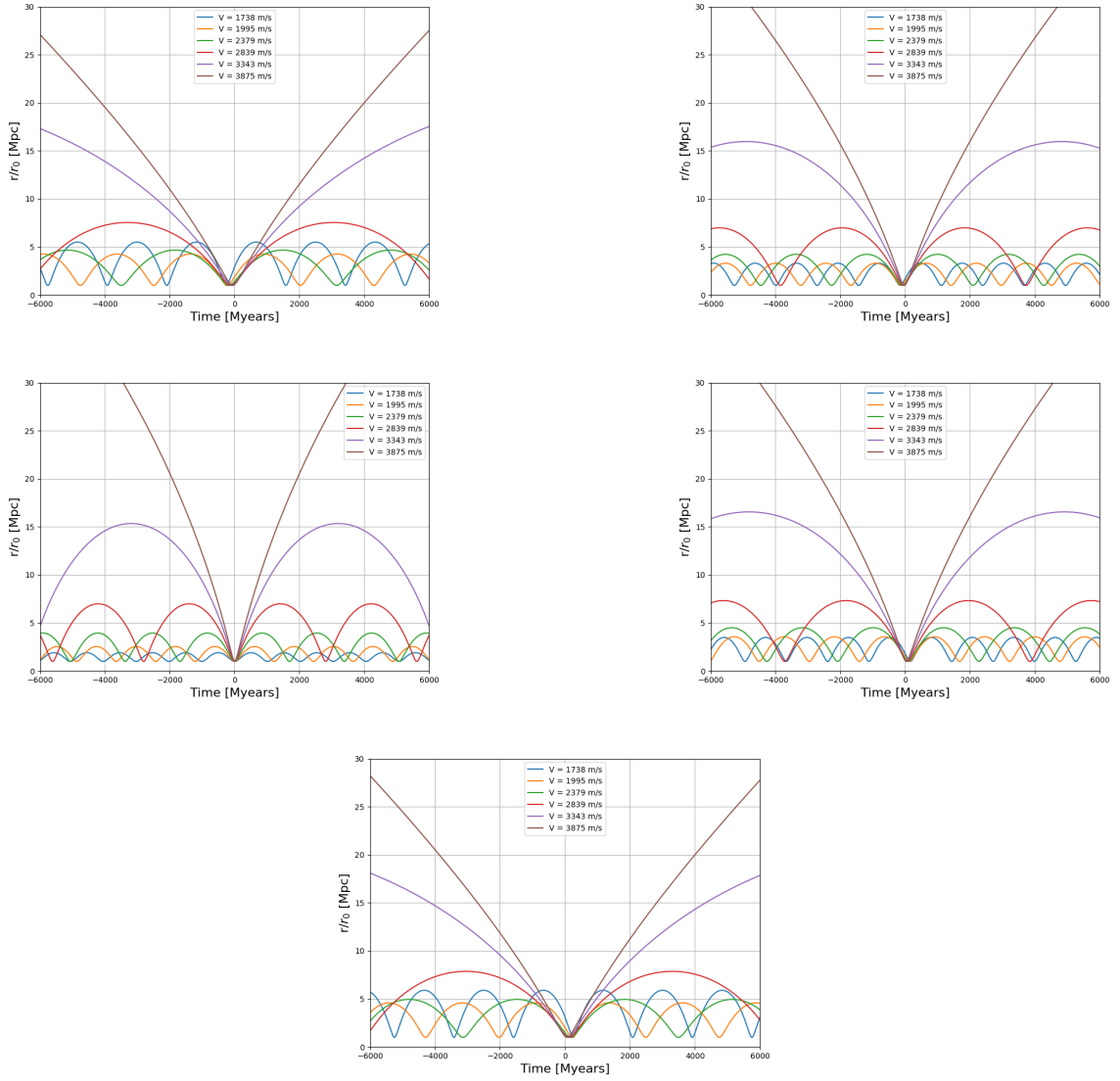

Figure 4.14: D100: the evolution of the deprojected radial distance in units of the pericenter distance for orbits with z_0 = (a) - 0.5 Mpc, (b) -0.25 Mpc, (c) 0 Mpc, (d) 0.25 Mpc, (e) 0.5 Mpc.

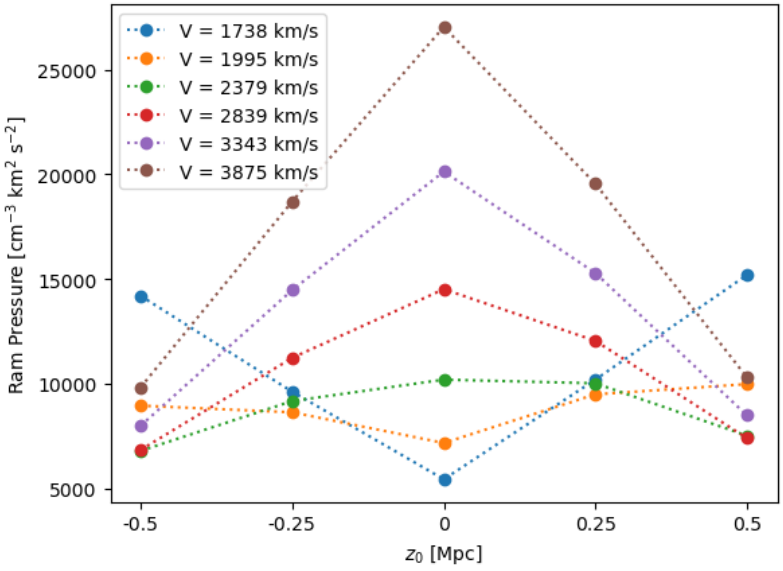

Figure 4.15: Dependence of peak of ram pressure on distance z_0 for various velocities for D100

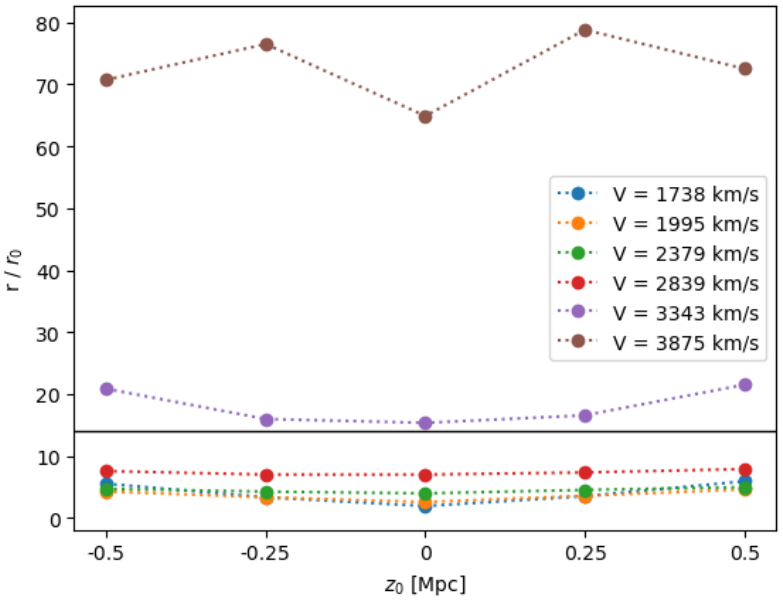

Figure 4.16: D100: dependence of pericentric to apocentric ratio on intial line- of-sight distance z_0. The horizontal line shows value 14

From comparison of the model orbits of galaxy D100 presented in Figures 4.9 - 4.13 we can observe the following trends:

- For orbits with negative values of initial parameter z_0 (currently farther away from us than the cluster center), pericenter occurs sooner (before $T = 0$ Myear), while for orbits with positive z_0, pericenter occurs later (after $T = 0$ Myear). The galaxy is currently at pericenter for $z_0 = 0$ kpc (Fig. 4.11).

- The slowest orbits (V = 1700 - 2800 km s^{-1}) in most cases do not cross the virial radius of the cluster. The fastest orbit ($V \sim 3900$ km s^{-1}) is likely too elongated, only marginally bound to the cluster.

- The pericenter distances of the model orbits are in the range of about 0.25 - 0.6 Mpc. The times from/to pericenter are in the range 0 - 250 Myr, and within 150 Myr for the faster orbits.

- Figure 4.15, that plots the peak of ram pressure as a function of z_0, shows the following trend. For higher velocities (V = 2400 - 3900 km s^{-1}), ram pressure peak is the highest for $z_0 = 0$ kpc and nearly symetrically decreases for positive and also negative z_0. The trend is opposite for smaller velocities (V = 1700 - 2000 km s^{-1}) which however are unlikely due to their compact shapes. For velocity between V = 2000 - 2400 km s^{-1}, the peak ram pressure does not change much with z_0. For $z_0 = 0$ kpc, the peak values of ram pressure for faster orbits ($V > 2800$ km s^{-1}) are $\sim 15,000 - 27,000$ cm^{-3}(km/s)^2.

- Fig. 4.16 plots the values of the ratio of the apocenter to pericenter distances for orbits with different z_0 and initial velocities. The orbits of infalling galaxies in cosmological N-body simulations have mostly a ratio $r_{\rm apo}/r_{\rm peri}$ about 14. The plot in Fig. 4.16 shows that the fastest modeled orbit ($V = 3900$ km s^{-1}) has the ratio too high. For the second highest velocity ($V = 3300$ km s^{-1}) the ratio consistent in the range of z_0 from -250 to 250 kpc. As expected, the four remaining velocities (V = 1700 - 2800 km s^{-1}) have the ratio too low and nearly independent of z_0. There is also a trend - the ratio is the smallest for $z_0 = 0$ kpc, then it behaves symmetrically for both (positive and negative) z_0.

- From modeled orbits we can specify that the lower limit of possible velocities is about $V = 3000$ km s^{-1}. From the apocenter to pericenter ratio we can say that that the top limit of possible velocities is somewhere between 3300 km s^{-1} - 3900 km s^{-1}, because the orbit with V = 3900 km s^{-1} has the ratio too high. For velocity 3300 km s^{-1}, more probable values of z_0 are in range of -250 kpc to 250 kpc. The most probable orbit is the one with $V = 3300$ km s^{-1} for z_0 from -250 to 250 kpc.

4.3 Discussion and Comparison of NGC 4858 and D100

Now, we will compare results for both galaxies and discuss them.

- Lower limit of possible velocities for both galaxies is about 3000 km s^{-1}. The top limit for D100 is between 3300 km s^{-1} and 3900 km s^{-1}, for NGC 4858 it is something more than 3400 km s^{-1}. These values are summarized in table 4.1.

- Dependence of ram pressure on distance z_0 is different for both galaxies. Dependence of apocentre to pericentre distance on z_0 is also different for both galaxies.

- Dependence of pericenter on the initial distance z_0 comes out vice versa for both galaxies.

Table 4.1: Lower and top possible velocities for galaxies D100 and NGC 4858.

galaxy	V_{min} [km s^{-1}]	V_{max} [km s^{-1}]
D100	3000	3300 - 3900
NGC 4858	3000	> 3400

Despite the differences in the observed orbital (fixed) parameters of the two galaxies, our modeling suggested that they both are at orbits with currently high deprojected velocities > 3000 km s^{-1}. Such velocities are considerably larger than the velocity dispersion of the Coma cluster galaxies ($\sigma \sim 1000$ km s^{-1}). This indicates that the high orbital velocity might be the main reason why the two galaxies are strongly affected by ram pressure and thus are in fact jellyfish galaxies.

D100 is projected closer to the cluster center than NGC 4858, as we can see from Fig. 4.17. The Figure also illustrates that the tail of D100 has a much more tangential direction relative to the cluster center than radial. The tail is nearly perpendicular to the direction to the cluster center (see table 4.2). D100 also has a smaller line-of-sight velocity than NGC 4858.

Together with the results of our modeling, this indicates that D100 is likely close to the pericenter or almost in pericenter, and has been experiencing strong ram pressure over the last couple of hundreds of Myr.

For NGC 4858, our modeling showed that here is a strong difference in the (near) future depending on the galaxy's current z_0 position. The apocentric-to-pericentric ratio analysis indicated that negative z_0's are more likely. Thus, the galaxy probably will experience a strong increase in RP in the coming ~ 200 Myr.

These results are consistent with the great difference in the observed morphology of both galaxies and their tails (see Figures 2.6, 2.7, 3.1 (right panel) and 3.2). NGC 4858 has a relatively extended gas disk, thus not yet strongly stripped, and the tail is wide. In comparison, the gas disk of D100 is significantly smaller, and its tail is longer and much narrower. All this indicates that D100 is in a late stage of ram pressure stripping, while NGC 4858 in an earlier stage of stripping.

As stated in Section 2.3.1, the gravitational restoring force of the galaxy is an important factor in the effects of ram pressure stripping. Since both the galaxies have similar masses ($M_* \sim 2 \times 10^9\ M_\odot$), the differences observed in their stripping stages must be related to the parameters of their orbits, mainly to the different stage along the orbits.

Table 4.2: Comparison of parameters for galaxies NGC 4858 and D100. (source: https://simbad.u-strasbg.fr/simbad/)

Galaxy	Projected distance from cluster center [kpc]	Line-of-sight velocity [km s^{-1}]	Direction of tail relative to cluster centre [°]
NGC 4858	380	2336	128
D100	240	-1665	94

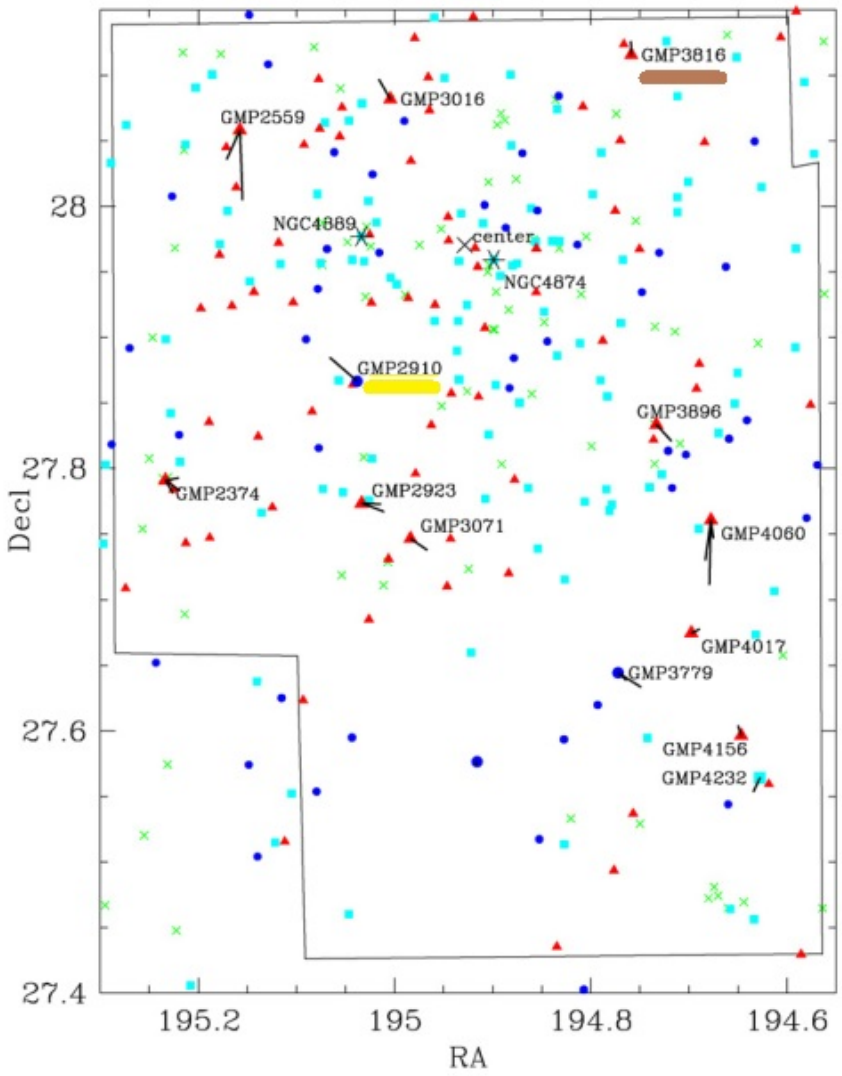

Figure 4.17: Known jellyfish galaxies in the Coma cluster. Our sample galaxies are the marked ones: GMP 2910 (D100) - yellow, GMP 3816 (NGC 4858) - brown. The black lines mark the direction of jellyfish tails and the colour and shape distribution correspond to redshift. Source: Yagi et al. 2010.

Chapter 5

Conclusion

In our work we studied and analyzed the orbits of the jellyfish galaxies NGC 4858 and D100 in the Coma cluster. The gravitational potential of the cluster was modeled by Navarro-Frenk-White profile. We developed a Python script to semi-analytically model the orbits. Using the initial conditions, we varied the free parameters in order to model 20 orbits for each galaxy. These orbits are all consistent with the current observed fixed parameters. In order to follow the orbits to both directions from the initial location (to the past and the future), we ran two executions of the model, one with positive, and another with negative time step. We plotted the projections of the orbits and the evolution of their deprojected orbital velocity, deprojected distance from the cluster centre and the ram pressure that the galaxies experienced along the orbits. We described the principal parameters of the orbits, such as the pericentric distance, time to/from pericenter, learned about the ram pressure history along the orbits, and with help of the suggestions of the cosmological simulations, we limited the range of possible orbits. In the following paragraphs, we summarize our results.

For galaxy NGC 4858, we estimated the lower limit of possible velocities $V = 3000\,\mathrm{km\,s^{-1}}$ and the top limit $V = 3400$ - $3000\,\mathrm{km\,s^{-1}}$. The most probable orbits for this galaxy are the ones with $\mathrm{V} = 3000\,\mathrm{km\,s^{-1}}$ and negative z_0. At those orbits, the galaxy is currently before the closest approach to the cluster center. It means that NGC 4858 will probably shortly experience a steep increase in ram pressure stripping.

For D100, similarly to NGC4858, the lower limit of possible velocities is also about $V = 3000\,\mathrm{km\,s^{-1}}$ and the top limit is somewhere between $V = 3400$ - $3800\,\mathrm{km\,s^{-1}}$. The most probable orbits for this galaxy are the ones with $\mathrm{V} = 3000\,\mathrm{km\,s^{-1}}$ for z_0 from the range -250 kpc to 250 kpc, possibly close to 0 kpc. At such orbits, the galaxy is close to pericenter, and thus it has been recently experiencing a strong ram pressure stripping.

Thus we conclude that both of these galaxies are at orbits with $V > 3000\,\mathrm{km\,s^{-1}}$. Such velocities are larger than the velocity dispersion of the Coma cluster galaxies ($\sigma\ \sim$1000 $\mathrm{km\,s^{-1}}$). This might explain the substantial effects of ram pressure stripping of the galaxies and consequently their jellyfish appearance.

For galaxy D100, the pericenter distances along the modeled orbits are in the range of about 0.25 - 0.6 Mpc. The times from/to pericenter are in the range 0 -

250 Myr, and within 150 Myr for the faster orbits. For NGC 4858, the pericenter distances are in the range of about 0.3 - 0.5 Mpc, while the times from/to pericenter are in the range 0 - 200 Myr.

Bibliography

Boselli, Alessandro, Matteo Fossati, and Ming Sun (2022). "Ram pressure stripping in high-density environments". In: 30.1, 3, p. 3. DOI: 10.1007/s00159-022-00140-3. arXiv: 2109.13614 [astro-ph.GA].

Brilenko, R. D., M. V. Eingorn, and A. I. Zhuk (2017). "Dark and visible matter distribution in Coma cluster: theory vs observations". In: *Astronomical and Astrophysical Transactions* 30.1, pp. 81–94.

Cramer, W. J. et al. (2019). "Spectacular Hubble Space Telescope Observations of the Coma Galaxy D100 and Star Formation in Its Ram Pressure-stripped Tail". In: 870.2, 63, p. 63. DOI: 10.3847/1538-4357/aaefff. arXiv: 1811.04916 [astro-ph.GA].

Fossati, Matteo et al. (2012). "65 kpc of ionized gas trailing behind NGC 4848 during its first crossing of the Coma cluster". In: 544, A128, A128. DOI: 10.1051/0004-6361/201219933. arXiv: 1207.4806 [astro-ph.CO].

Gunn, James E. and III Gott J. Richard (1972). "On the Infall of Matter Into Clusters of Galaxies and Some Effects on Their Evolution". In: 176, p. 1. DOI: 10.1086/151605.

Jáchym, Pavel et al. (2017). "Molecular Gas Dominated 50 kpc Ram Pressure Stripped Tail of the Coma Galaxy D100". In: 839.2, 114, p. 114. DOI: 10.3847/1538-4357/aa6af5. arXiv: 1704.00824 [astro-ph.GA].

Köppen, J. et al. (2018). "Ram pressure stripping made easy: an analytical approach". In: 479.4, pp. 4367–4390. DOI: 10.1093/mnras/sty1610. arXiv: 1806.05887 [astro-ph.GA].

Kubo, Jeffrey M. et al. (2007). "The Mass of the Coma Cluster from Weak Lensing in the Sloan Digital Sky Survey". In: 671.2, pp. 1466–1470. DOI: 10.1086/523101. arXiv: 0709.0506 [astro-ph].

Roberts, Ian D. and Laura C. Parker (2020). "Ram pressure stripping candidates in the coma cluster: evidence for enhanced star formation". In: 495.1, pp. 554–569. DOI: 10.1093/mnras/staa1213. arXiv: 2004.12033 [astro-ph.GA].

Wetzel, Andrew R. (2011). "On the orbits of infalling satellite haloes". In: 412.1, pp. 49–58. DOI: 10.1111/j.1365-2966.2010.17877.x. arXiv: 1001.4792 [astro-ph.CO].

Yagi, Masafumi et al. (2010). "A Dozen New Galaxies Caught in the Act: Gas Stripping and Extended Emission Line Regions in the Coma Cluster". In: 140.6, pp. 1814–1829. DOI: 10.1088/0004-6256/140/6/1814. arXiv: 1005.3874 [astro-ph.CO].

Zadorozhna, L. et al. (2023). "The study of x-ray spectrum of the Coma cluster". In: *arXiv e-prints*, arXiv:2311.08603, arXiv:2311.08603. DOI: 10.48550/arXiv.2311.08603. arXiv: 2311.08603 [astro-ph.CO].